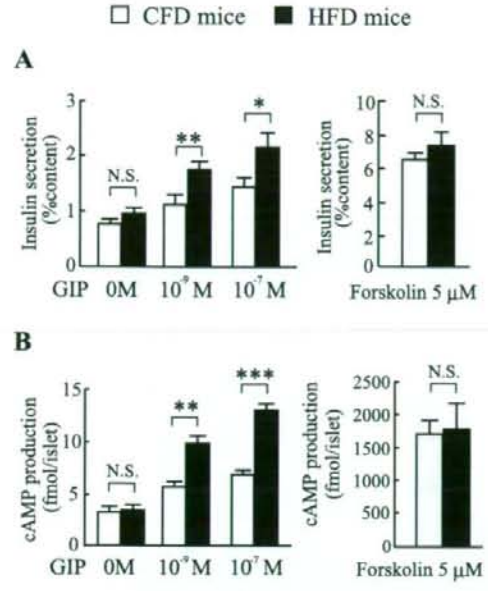

Fig. 5. Insulin secretion and cAMP production induced by GIP in isolated islets of CFD and HFD mice.Insulin secretion ($n = 10$; *A*) and intracellular cAMP levels ($n = 6$; *B*) in isolated islets of CFD (open bars) and HFD mice (filled bars) were examined in response to 10^{-9} or 10^{-7} M GIP in the presence of 11.1 mM glucose. The isolated islets of these mice were incubated with 5 μM forskolin to assess maximal insulin secretion and cAMP production. Values are means ± SE. $*P < 0.05$, $**P < 0.01$, and $***P < 0.001$ vs. CFD mice.

We (21) previously investigated GIP-induced insulin secretion using *GIPR*$^{-/-}$ mice under high-fat feeding. The plasma insulin levels after meal ingestion were increased in high-fat diet-fed *GIPR*$^{+/+}$ mice compared with those in control diet-fed *GIPR*$^{+/+}$ mice, resulting in similar glucose levels. However, the postprandial glucose levels were increased by the lack of GIP-induced compensatory insulin secretion in high-fat diet-fed *GIPR*$^{-/-}$ mice, suggesting that increased insulin secretion due to enhanced GIP signaling is required to maintain glucose homeostasis in the obese state. In the present study, we have demonstrated hypersensitivity of GIPR to GIP in β-cells of high-fat-induced obese mice. Increased sensitivity of GIPR to GIP might result from increased expression of GIPR or hypersensitivity of intracellular GIP signal transduction. Some (9, 18) studies have reported that GIPR expression is an important factor in altering the GIP sensitivity of β-cells. In the study of diabetic Zucker fatty rats, GIPR mRNA expression and protein

Table 1. *Insulin secretion induced by glucose and high potassium (30 mM KCl) in the isolated islets of CFD and HFD mice*

%Content	CFD Mice	HFD Mice	*P* Value
2.8 mM glucose	0.69±0.21	0.68±0.07	NS
2.8 mM glucose + high potassium	0.99±0.12	1.00±0.17	NS
11.1 mM glucose	1.12±0.14	1.22±0.10	NS
11.1 mM glucose + high potassium	2.14±0.25	2.42±0.34	NS

Values are means ± SE; CFD (mice fed control fat chow; $n = 5$–6) vs. HFD mice (mice fed high-fat chow; $n = 5$–6). NS, not significant.

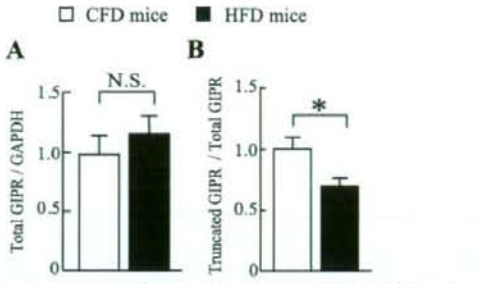

Fig. 6. Total and truncated GIPR expression in islets of CFD and HFD mice. Quantitative RT-PCR of total GIPR (*A*) and truncated GIPR (*B*) were assessed in islets of CFD ($n = 6$) and HFD mice ($n = 6$). The ratio of truncated GIPR to total GIPR (*B*) was calculated by quantitative RT-PCR of total GIPR and truncated GIPR. The data on HFD mice are shown relative to CFD mice. Values are means ± SE. $*P < 0.05$ vs. CFD mice.

were decreased in islets compared with that of lean rats, which led to diminished GIPR sensitivity to GIP (17). Here, we found that total GIPR expression was not decreased and that GIPR sensitivity to GIP was increased in isolated islets of our HFD mice due to decreased expression of truncated GIPR, in contrast to the findings in diabetic obese rats. Our HFD mice were mild obese and mild hyperinsulinemia induced by high-fat feeding rather than by genetic factors. In addition, our obese mice did not have diabetes. Thus, differences of the expression of GIPR and subsequent GIPR sensitivity to GIP may be due to the different phenotypes of diabetic obese rats and HFD mice.

We had previously obtained the extra band of this GIPR variant as well as the band of wild-type GIPR when we amplified mouse islet cDNA to detect wild-type GIPR using NH_2-terminal and COOH-terminal primers of GIPR. We analyzed the cDNA sequence of the extra band and identified it as a splice variant of GIPR that was not produced by PCR error. Indeed, certain GIPR splice variants resulting in truncation have been reported in previous studies (7, 32). These splice variants were detected from cDNA libraries of human islets and insulinoma. However, the variants were not examined in regard to their regulatory role in GIPR sensitivity. In the present study, by evaluating the function of truncated GIPR in transfected COS-7 cells, we have shown that truncated GIPR has a dose-dependent dominant negative effect against wild-type GIPR.

GPCRs were generally thought to function as monomers, but recent studies (5, 12, 13) have reported that GPCRs can form homodimeric or heterodimeric complexes with receptors in the ER and that these complexes are important in receptor folding and trafficking to the plasma membrane. In the present study, we investigated the mechanism of negative action of truncated GIPR against wild-type GIPR function using immunochemistry and immunoprecipitation of cotransfected cells. Truncated GIPR interacted with wild-type GIPR in the ER and influenced wild-type receptor trafficking to the cell membrane. Some GPCRs have specific motifs for dimerization that are required for transport of the receptors from the ER to the cell surface (1, 8, 19, 26). Mutations in these motifs prevent dimerization with wild-type receptors and inhibit their trafficking to the cell membrane, indicating a dominant negative effect against the wild-type receptor (19, 26). Although these specific motifs are

not found in GIPR, truncated GIPR might have formed from complexes with wild-type GIPR in our experiments.

To evaluate the functional relevance of truncated GIPR in vivo, we investigated the expression of truncated GIPR in β-cells. The relative abundance of truncated GIPR expression was decreased in islets of HFD mice. The decreased dominant negative effect due to reduced expression of truncated GIPR might well be involved in augmented intracellular cAMP production and insulin secretion in response to GIP in islets in diet-induced obesity. Altered selective splicing in response to metabolic changes of the insulin receptor in β-cells was also reported (10), and hyperglycemia not only decreased total insulin receptor expression but also altered the relative expression ratio of the two insulin receptor isoforms in human islets, resulting in attenuation of insulin signal transduction. Although the mechanism of mRNA selective splicing of GIPR is unclear, insulin is reported (4) to influence the activity of the mRNA slicing regulator ASF/SF2, a serine/arginine-rich protein (SR protein). Further study is necessary to clarify the mechanism of GIPR mRNA selective splicing in response to metabolic changes.

In conclusion, we have identified a splice variant GIPR in mouse islets that has a dominant negative effect against the wild-type receptor by interacting in translocation of wild-type GIPR from the ER to the cell surface. Thus, reduced expression of truncated GIPR due to selective splicing and subsequent GIPR hypersensitivity to GIP may be involved in increased insulin secretion in response to GIP in metabolic states such as obesity.

ACKNOWLEDGMENTS

We thank K. Yamada and Dr. M. Sasaki for technical help.

GRANTS

This study was supported by Scientific Research Grants from the Ministry of Education, Culture, Sports, Science, and Technology (Japan); Health and Labor Sciences Research Grants for Comprehensive Research on Aging and Health from the Ministry of Health, Labor, and Welfare (Japan); and the 21st Century Center of Excellence Program (Japan).

REFERENCES

1. **Andersson H, D'Antona AM, Kendall DA, Von Heijne G, Chin CN.** Membrane assembly of the cannabinoid receptor 1: impact of a long N-terminal tail. *Mol Phamacol* 64: 570–577, 2003.
2. **Boylan MO, Jepeal LI, Wolfe MM.** Structure of the rat glucose-dependent insulinotropic polypeptide receptor gene. *Peptides* 20: 219–228, 1999.
3. **Creuzfeldt W, Ebert R, Willms B, Frerichs H, Brown JC.** Gastric inhibitory polypeptide (GIP) and insulin in obesity: increased response to stimulation and defective feedback control of serum levels. *Diabetologia* 14: 15–24, 1983.
4. **Diamond RH, Du K, Lee VM, Mohn KL, Haber BA, Tewari DS, Taub R.** Novel delayed-early and highly insulin-induced growth response genes. Identification of HRS, a potential regulator of alternative pre-mRNA splicing. *J Biol Chem* 268: 15185–15192, 1993.
5. **Duvernay MT, Filipeanu CM, Wu G.** The regulatory mechanisms of export trafficking of G protein-coupled receptors. *Cell Signal* 17: 1457–1465, 2005.
6. **Flatt PR, Bailey CJ, Kwasowski P, Swanston-Flatt SK, Marks V.** Abnormalities of GIP in spontaneous syndromes of obesity and diabetes in mice. *Diabetes* 32: 433–435, 1983.
7. **Gremlich S, Porret A, Hani EH, Cherif D, Vionnet N, Froguel P, Thorens B.** Cloning, functional expression, and chromosomal localization of the human pancreatic islet glucose-dependent insulinotropic polypeptide receptor. *Diabetes* 44: 1202–1208, 1995.
8. **Hague C, Uberti MA, Chen Z, Hall RA, Minneman KP.** Cell surface expression of α_{1D}-adrenergic receptors is controlled by heterodimerization with α_{1B}-adrenergic receptors. *J Biol Chem* 279: 15541–15549, 2004.
9. **Holst JJ, Gromada J, Nauck MA.** The pathogenesis of NIDDM involves a defective expression of the GIP receptor. *Diabetologia* 40: 984–986, 1997.
10. **Hribal ML, Perego L, Lovari S, Andreozzi F, Menghini R, Perego C, Finzi G, Usellini L, Placidi C, Capella C, Guzzi V, Lauro D, Bertuzzi F, Davalli A, Pozza G, Pontiroli A, Federici M, Lauro R, Brunetti A, Folli F, Sesti G.** Chronic hyperglycemia impairs insulin secretion by affecting insulin receptor expression, splicing, and signaling in RIN beta cell line and human islets of Langerhans. *FASEB J* 17: 1340–1342, 2003.
11. **Ishihara T, Nakamura S, Kaziro Y, Takahashi T, Takahashi K, Nagata S.** Molecular cloning and expression of a cDNA encoding the secretin receptor. *EMBO J* 7: 1635–1641, 1991.
12. **Jones KA, Tamm JA, Craig DA, Durkin MM, Dai M, Yao WJ, Johnson M, Gunwaldsen C, Huang LY, Tang C, Shen Q, Salon JA, Morse K, Laz T, Smith KE, Nagarathnam D, Noble SA, Branchek TA, Gerald C.** GABA(B) receptors function as a heteromeric assembly of the subunits GABA(B)R1 and GABA(B)R2. *Nature* 396: 674–679, 1998.
13. **Jordan BA, Trapaidze N, Gomes I, Nivarthi R, Devi LA.** Oligomerization of opioid receptors with β_2-adrenergic receptors: a role in trafficking and mitogen-activated protein kinase activation. *Proc Natl Acad Sci USA* 98: 343–348, 2001.
14. **Kahn BB, Flier JS.** Obesity and insulin resistance. *J Clin Invest* 106: 473–481, 2000.
15. **Kubota A, Yamada Y, Hayami T, Yasuda K, Someya Y, Ihara Y, Kagimoto S, Watanabe R, Taminato T, Tsuda K, Seino Y.** Identification of two missense mutations in the GIP receptor gene: a functional study and association analysis with NIDDM: no evidence of association with Japanese NIDDM subjects. *Diabetes* 45: 1701–1705, 1996.
16. **Lemieux I, Pascot A, Couillard C, Lamarche B, Tchernof A, Alméras N, Bergeron J, Gaudet D, Tremblay G, Prud'homme D, Nadeau A, Després JP.** Hypertriglyceridemic waist: A marker of the atherogenic metabolic triad (hyperinsulinemia; hyperapolipoprotein B; small, dense LDL) in men? *Circulation* 102: 179–184, 2000.
17. **Lynn FC, Pamir N, Ng EH, McIntosh CH, Kieffer TJ, Pederson RA.** Defective glucose-dependent insulinotropic polypeptide receptor expression in diabetic fatty Zucker rats. *Diabetes* 50: 1004–1011, 2001.
18. **Lynn FC, Thompson SA, Pospisilik JA, Ehses JA, Hinke SA, Pamir N, McIntosh CH, Pederson RA.** A novel pathway for regulation of glucose-dependent insulinotropic polypeptide (GIP) receptor expression in beta cells. *FASEB J* 17: 91–93, 2003.
19. **Margeta-Mitrovic M, Jan YN, Jan LY.** Function of GB1 and GB2 subunits in G protein coupling of GABA(B) receptors. *Proc Natl Acad Sci USA* 98: 14649–14654, 2001.
20. **Miyawaki K, Yamada Y, Ban N, Ihara Y, Tsukiyama K, Zhou H, Fujimoto S, Oku A, Tsuda K, Toyokuni S, Hiai H, Mizunoya W, Fushiki T, Holst JJ, Makino M, Tashita A, Kobara Y, Tsubamoto Y, Jinnouchi T, Jomori T, Seino Y.** Inhibition of gastric inhibitory polypeptide signaling prevents obesity. *Nat Med* 8: 738–742, 2002.
21. **Miyawaki K, Yamada Y, Yano H, Niwa H, Ban N, Ihara Y, Kubota A, Fujimoto S, Kajikawa M, Kuroe A, Tsuda K, Hashimoto H, Yamashita T, Jomori T, Tashiro F, Miyazaki J, Seino Y.** Glucose intolerance caused by a defect in the entero-insular axis: a study in gastric inhibitory polypeptide receptor knockout mice. *Proc Natl Acad Sci USA* 96: 14843–14847, 1999.
22. **Mukai E, Ishida H, Kato S, Tsura Y, Fujimoto S, Takahashi A, Horie M, Tsuda K, Seino Y.** Metabolic inhibition impairs ATP-sensitive K^+ channel block by sulfonylurea in pancreatic β-cells. *Am J Physiol Endocrinol Metab* 274: E38–E44, 1998.
23. **Nakamura Y, Suzuki H, Sakaguchi M, Mihara K.** Targeting and assembly of mitochondrial translocase of outer membrane 22 (TOM22) into the TOM complex. *J Biol Chem* 279: 21223–21232, 2004.
24. **Pederson RA.** GIP. *Gut Peptides*, edited by Walsh J and Dockray G. New York: Raven, 1993, p. 217–259.
25. **Reaven GM.** Role of insulin resistance in human disease. *Diabetes* 37: 1066–1084, 1988.
26. **Salahpour A, Angers S, Mercier JF, Lagace M, Marullo S, Bouvier M.** Homodimerization of the β2-adrenergic receptor as a prerequisite for cell surface targeting. *J Biol Chem* 279: 33390–33397, 2004.
27. **Service FJ, Rizza RA, Westland RE, Hall LD, Gerich JE, Go VL.** Gastric inhibitory polypeptide in obesity and diabetes mellitus. *J Clin Endocrinol Metab* 58: 1133–1140, 1984.

28. **Stock S, Leichner P, Wong AC, Ghatei MA, Kieffer TJ, Bloom SR, Chanoine JP.** Ghrelin, peptide YY, glucose-dependent insulinotropic polypeptide, and hunger responses to a mixed meal in anorexic, obese, and control female adolescents. *J Clin Endocrinol Metab* 90: 2161–2168, 2005.
29. **Sutton R, Peters M, McShane P, Gray DW, Morris PJ.** Isolation of rat pancreatic islets by ductal injection of collagenase. *Transplantation* 42: 689–691, 1986.
30. **Tsukiyama K, Yamada Y, Yamada C, Harada N, Kawasaki Y, Ogura M, Bessho K, Li M, Amizuka N, Sato M, Udagawa N, Takahashi N, Tanaka K, Oiso Y, Seino Y.** Gastric inhibitory polypeptide as an endogenous factor promoting new bone formation following food ingestion. *Mol Endocrinol* 20: 1644–1651, 2006.
31. **Usdin TB, Mezey E, Button DC, Brownstein MJ, Bonner TI.** Gastric inhibitory polypeptide receptor, a member of the secretin-vasoactive intestinal peptide receptor family, is widely distributed in peripheral organs and the brain. *Endocrinology* 133: 2861–2870, 1993.
32. **Volz A, Göke R, Lankat-Buttgereit B, Fehmann HC, Bode HP, Goke B.** Molecular cloning, functional expression, and signal transduction of the GIP-receptor cloned from a human insulinoma. *FEBS Lett* 373: 23–29, 1995.
33. **Yamada Y, Hayami T, Nakamura K, Kaisaki PJ, Someya Y, Wang CZ, Seino S, Seino Y.** Human gastric inhibitory polypeptide receptor: cloning of the gene (GIPR) and cDNA. *Genomics* 29: 773–776, 1995.

Am J Physiol Lung Cell Mol Physiol 295: L698–L707, 2008.
First published August 1, 2008; doi:10.1152/ajplung.90352.2008.

Aberrant catalytic cycle and impaired lipid transport into intracellular vesicles in ABCA3 mutants associated with nonfatal pediatric interstitial lung disease

Yoshihiro Matsumura,[1] Nobuhiro Ban,[1,2] and Nobuya Inagaki[1,2]

[1]*Department of Physiology, Akita University School of Medicine, Akita; and* [2]*Department of Diabetes and Clinical Nutrition, Graduate School of Medicine, Kyoto University, and Core Research for Evolutional Science and Technology of Japan Science and Technology Agency, Kyoto, Japan*

Submitted 18 June 2008; accepted in final form 31 July 2008

Matsumura Y, Ban N, Inagaki N. Aberrant catalytic cycle and impaired lipid transport into intracellular vesicles in ABCA3 mutants associated with nonfatal pediatric interstitial lung disease. *Am J Physiol Lung Cell Mol Physiol* 295: L698–L707, 2008. First published August 1, 2008; doi:10.1152/ajplung.90352.2008.—The ATP-binding cassette transporter ABCA3 mediates uptake of cholinephospholipids into intracellular vesicles and is essential for surfactant metabolism in lung alveolar type II cells. We have shown previously that *ABCA3* mutations in fatal surfactant deficiency impair intracellular localization or ATP hydrolysis of ABCA3 protein. However, the mechanisms underlying the less severe phenotype of patients with *ABCA3* mutation are unclear. In this study, we characterized ABCA3 mutant proteins identified in pediatric interstitial lung disease (pILD). E292V (intracellular loop 1), E690K (adjacent to Walker B motif in nucleotide binding domain 1), and T1114M (8th putative transmembrane segment) mutant proteins are localized mainly in intracellular vesicle membranes as wild-type protein. Lipid analysis and sucrose gradient fractionation revealed that the transport function of E292V mutant protein is moderately preserved, whereas those of E690K and T1114M mutant proteins are severely impaired. Vanadate-induced nucleotide trapping and photoaffinity labeling of wild-type and mutant proteins using 8-azido-[^{32}P]ATP revealed an aberrant catalytic cycle in these mutant proteins. These results demonstrate the importance of a functional catalytic cycle in lipid transport of ABCA3 and suggest a pathophysiological mechanism of pILD due to *ABCA3* mutation.

ATP-binding cassette A3 mutant; pediatric interstitial lung disease; lamellar body; lipid transporter; phosphatidylcholine

THE FAMILY OF ATP-BINDING CASSETTE (ABC) transporters is involved in ATP-dependent transport of various substrates across membranes (14). ABCA3 is expressed predominantly at the limiting membrane of the lamellar bodies in lung alveolar type II cells and is proposed to be a surfactant lipid transporter (20, 36). Exogenous expression of ABCA3 in cultured cells promotes lipid uptake into intracellular vesicles that generate lamellar body-like vesicles (7, 18, 21). ABCA3 deficiency in human and mice leads to decreased phosphatidylcholine and phosphatidylglycerol in surfactant, dysgenesis of lamellar bodies, and respiratory distress (1, 3, 8, 11, 12, 27). Considered together, these results indicate that ABCA3 is an essential lipid transporter in surfactant metabolism.

In addition, *ABCA3* mutations cause lung disease of differing severity. We previously found that *ABCA3* mutations in fatal surfactant deficiency can result in abnormal intracellular localization (type I) or impaired ATP hydrolysis of ABCA3 protein (type II) (17). For example, patients with type I homozygous *ABCA3* mutations such as W1142X/W1142X or type I/type II compound heterozygous *ABCA3* mutations such as L982P/G1221S die of surfactant deficiency within the neonatal period (27). On the other hand, patients with the common missense mutation E292V and a second, specific mutation such as E690K or T1114M develop pediatric interstitial lung disease (pILD), the phenotype of which is milder than that of fatal surfactant deficiency, suggesting that the E292V *ABCA3* mutation is responsible for the development of pILD (4). However, the mechanism underlying the phenotypic heterogeneity of lung disease associated with *ABCA3* mutation remains unknown.

In this study, we characterized E292V, E690K, and T1114M mutant ABCA3 proteins identified in pILD. Analysis of these ABCA3 mutants demonstrates the importance of a functional catalytic cycle in the lipid transport function of ABCA3 and suggests various therapeutic targets in lung disease due to *ABCA3* mutation.

MATERIALS AND METHODS

DNA construction. The plasmid pEGFPN1-ABCA3 (17), which encodes ABCA3 protein fused with enhanced green fluorescent protein (GFP) at the COOH terminus (ABCA3-GFP), and its mutants containing pILD mutations (E292V, E690K, and T1114M) and other site-directed mutations (E292D, E292K, T1114S, E690D, and E690R) were generated as described previously and used for transient transfection experiment. Plasmid pCAGIpuro-ABCA3-GFP (17), which encodes ABCA3-GFP and its mutants described above, driven by a CAG promoter containing an internal ribosomal entry site and puromycin *N*-acetyltransferase gene cassette (22), was generated as described previously and used for stable transfection experiments.

Confocal microscopy. Human embryonic kidney (HEK-293) cells were grown at 37°C under 5% CO_2 in Dulbecco's modified Eagle's medium (Sigma) supplemented with 10% fetal calf serum and penicillin/streptomycin. HEK-293 cells (3×10^5) were seeded into 35-mm dishes with a poly-L-lysine-coated cover glass. After 24 h, HEK-293 cells were transfected with wild-type or mutant pEGFP plasmid (1 μg) using FuGENE transfection reagent (Roche Applied Science). The transfected cells were cultured for 48 h, fixed with 4% paraformaldehyde, and viewed with a Zeiss confocal microscope LSM510-META.

Glycosylation of ABCA3-GFP and mutant proteins. HEK-293 cells (3×10^6) were seeded into 100-mm dishes 24 h before transfection. Forty-eight hours after transfection with pEGFP vectors (6.25 μg) using FuGENE reagent, the cells were homogenized in 50 mM Tris·HCl buffer (pH 7.5) containing Complete protease inhibitor mixture (Roche Applied Science), and the total membrane fraction

Address for reprint requests and other correspondence: N. Inagaki, Dept. of Diabetes and Clinical Nutrition, Graduate School of Medicine, Kyoto Univ., 54 Kawahara-cho, Shogoin, Sakyo-ku, Kyoto 606-8507, Japan (e-mail: inagaki@metab.kuhp.kyoto-u.ac.jp).

The costs of publication of this article were defrayed in part by the payment of page charges. The article must therefore be hereby marked "*advertisement*" in accordance with 18 U.S.C. Section 1734 solely to indicate this fact.

(100,000-*g* pellet) was obtained as described previously (17). Ten micrograms of total membrane fraction were treated with 1 unit of peptide *N*-glycosidase F (PNGase F) or 5 milliunits of endoglycosidase H (Endo H) for 30 min at 37°C. The deglycosylated proteins were separated by SDS-PAGE and analyzed by immunoblot analysis using anti-GFP monoclonal antibody (Santa Cruz Biotechnology).

Establishment of HEK-293 cells stably expressing ABCA3-GFP and mutant proteins. HEK-293 cells (3×10^5) were seeded into 35-mm dishes and, after 24 h, transfected with linearized pCAGIpuro plasmids (1 μg) with *PvuI* using FuGENE reagent. Forty-eight hours after transfection, the cells were trypsinized, seeded into 100-mm dishes, and selected by 2.5 μg/ml puromycin for 7 days. Resistant colonies were combined and used for lipid analysis, whereas single colonies were isolated and used for nucleotide trapping and photoaffinity labeling experiments. The expression of ABCA3-GFP, LAMP3, and GRP78 was examined by immunoblot analysis using anti-GFP, anti-LAMP3 (Chemicon), and anti-GRP78 (Santa Cruz Biotechnology) antibodies, respectively.

Sucrose gradient fractionation. Confluent cells (five 100-mm dishes) were harvested and disrupted in 20 mM Tris·HCl buffer (pH 7.3) containing 1 M sucrose and Complete protease inhibitor mixture by N_2 cavitation, followed by centrifugation at 1,000 *g* for 10 min to obtain postnuclear supernatant (PNS). A sucrose gradient consisting of 1 ml each of 0.8, 0.7, 0.6, 0.5, 0.4, and 0.3 M sucrose and 0.5 ml of 0.2 M sucrose was layered successively above 3.5 ml of PNS (4 mg of protein). The gradient was spun in a P40ST rotor (Hitachi) at 125 *g* for 15 min and then at 80,000 *g* for 3 h. After centrifugation, 1 ml of each fraction was collected from the top.

Lipids analysis. Total lipids in PNS and sucrose gradient fractions were extracted using the method of Bligh and Dyer (2). The amount of total cholesterol and choline-phospholipids was measured using an enzymatic assay kit (Kyowa Medex and Wako, respectively). Data normalized by the protein content are represented as means ± SD, and statistical analysis was performed using the Bonferroni/Dunn procedure for post hoc testing.

Vanadate-induced nucleotide trapping of ABCA3-GFP and mutant proteins. A 20,000-*g* membrane fraction was obtained from HEK-293 cells stably expressing wild-type ABCA3-GFP or mutants as described previously (17). A 20,000-*g* membrane fraction (18–24 μg of protein) was incubated with 10 μM 8-azido-[α-^{32}P]ATP, 2 mM ouabain, 0.1 mM EGTA, 3 mM $MgCl_2$, and 40 mM Tris·HCl (pH 7.5) in a total volume of 12 μl for 10 min at 37°C in the presence or absence of 0.4 mM orthovanadate. In some experiments, 8-azido-[α-^{32}P]ATP was replaced with 8-azido-[γ-^{32}P]ATP. The reaction was stopped by adding 400 μl of ice-cold TEM buffer [40 mM Tris·HCl buffer (pH 7.5) containing 0.1 mM EGTA and 1 mM $MgCl_2$]. The supernatant containing unbound nucleotides was removed from the membrane pellet after centrifugation (20,000 *g*, 10 min, 2°C), and the procedure was repeated once. In the release experiment, following the initial removal of unbound nucleotides, the pellets were suspended in 100 μl of TEM buffer and incubated for 0–15 min at 37°C to release trapped nucleotides. After incubation, 300 μl of TEM buffer were added and supernatant containing released nucleotides was removed from the membrane pellet after centrifugation (20,000 *g*, 10 min, 2°C). The pellets were resuspended in 10 μl of TEM buffer and irradiated for 5 min (254 nm, 8.2 mW/cm^2) on ice. The samples were then electrophoresed on a 5% SDS-polyacrylamide gel and transferred to a polyvinylidene difluoride (PVDF) membrane (Millipore). The radioactivities of photoaffinity-labeled protein (total 220-kDa noncleaved form plus 180-kDa cleaved form) were quantified using FLA-5000 (Fujifilm). Radioactivities in the absence of orthovanadate were subtracted from radioactivities in the presence of orthovanadate and presented as means ± SD after normalization to the level of ABCA3-GFP protein (total 220-kDa noncleaved form plus 180-kDa cleaved form). Statistical analysis was performed as described above.

Photoaffinity labeling of ABCA3-GFP and mutant proteins with 8-azido-[γ-^{32}P]ATP or 8-azido-[α-^{32}P]ADP. A 20,000-*g* membrane fraction was incubated with 40 μM 8-azido-[γ-^{32}P]ATP or 8-azido-[α-^{32}P]ADP, 2 mM ouabain, 0.1 mM EGTA, 3 mM $MgCl_2$, and 40 mM Tris·HCl (pH 7.5) in a total volume of 12 μl for 10 min at 0°C. After irradiation for 5 min (254 nm, 8.2 mW/cm^2) on ice, 400 μl of TEM buffer were added and supernatant containing unbound nucleotides was removed from the membrane pellet after centrifugation (20,000 *g*, 10 min, 2°C). The pellets were solubilized in RIPA buffer [50 mM Tris·HCl (pH 7.5), 150 mM NaCl, 1 mM EDTA, 1% Nonidet P-40, 0.1% SDS, and 0.5% sodium deoxycholate] containing protease inhibitor mixture for 30 min at 4°C. After centrifugation (20,000 *g*, 20 min, 2°C), proteins were immunoprecipitated from the supernatant with the anti-human ABCA3 antibody (38). Samples were electrophoresed on a 5% SDS-polyacrylamide gel and transferred to a PVDF membrane. The radioactivities of photoaffinity-labeled protein (total 220-kDa noncleaved form plus 180-kDa cleaved form) were quantified using FLA-5000. To confirm the expression level of ABCA3-GFP proteins, the membrane was further analyzed by immunoblotting using anti-GFP antibody. Data normalized to the level of ABCA3-GFP proteins (total 220-kDa noncleaved form plus 180-kDa cleaved form) are presented as means ± SD. Statistical analysis was performed as described above.

Homology modeling of nucleotide binding domain 1 of ABCA3. The secondary structures of nucleotide binding domains (NBDs) of ABCA3 and other ABC transporters were predicted using the PSIPRED program (19). Amino acids sequences were aligned using the ClustalW program (15) and manually corrected based on the predicted secondary structures. The amino acids residues 545–766 in NBD-1 of ABCA3 share 29.7%, 25.7%, and 23.4% sequence identities with *Escherichia coli* maltose transporter MalK, *Staphylococcus aureus* Sav1866, and *E. coli* hemolysin transporter HlyB, respectively (6, 9, 39). The structure of NBD-1 of ABCA3 was modeled based on the ATP-bound closed form of *E. coli* MalK (Protein Data Bank entry 1Q12; Ref. 6) using SWISS-MODEL (26). Amino acid substitution was performed on Swiss-PDB Viewer, considering the best rotamer conformation.

RESULTS

Subcellular localization and glycosylation of ABCA3-GFP and pILD mutant proteins. We previously found that GFP-tagged wild-type ABCA3 protein (ABCA3-GFP) expressed in cultured cells is localized mainly at the limiting membrane of LAMP3-positive vesicles, whereas type I mutant protein (e.g., L101P) in fatal surfactant deficiency remains localized in the endoplasmic reticulum, accompanied by impaired processing of oligosaccharide (17). The E292V, E690K, and T1114M mutations identified in pILD (4) are located at intracellular loop 1 (ICL-1), adjacent to the Walker B motif in NBD-1 and the 8th putative transmembrane segment (TM-8), respectively (Fig. 1*A*). When E292V, E690K, and T1114M mutant ABCA3-GFP proteins were transiently expressed in HEK-293 cells, most of the GFP fluorescence was located at intracellular vesicles, as with the wild-type protein (Fig. 1*B*). ABCA3 is expressed as 190- and 150-kDa forms, with the latter suggested to be produced by proteolytic cleavage at extracellular domain 1 (ECD1) within lysosomal vesicles (21, 36). In native lung tissue, the cleaved form is predominant, whereas both forms are detected when overexpressed in cultured cells. Immunoblot analysis of total membrane fraction from transiently transfected HEK-293 cells using anti-GFP antibody showed two bands at ~220 kDa (noncleaved form) and 180 kDa (cleaved form) in wild-type and three mutant ABCA3-GFP proteins (Fig. 1*C*). In E690K mutant protein, the amount of the 180-kDa cleaved form was increased compared with that of wild-type protein. PNGase F digestion of total membrane fraction showed that the 220-kDa forms of all three mutants are *N*-glycosylated, as is wild-type

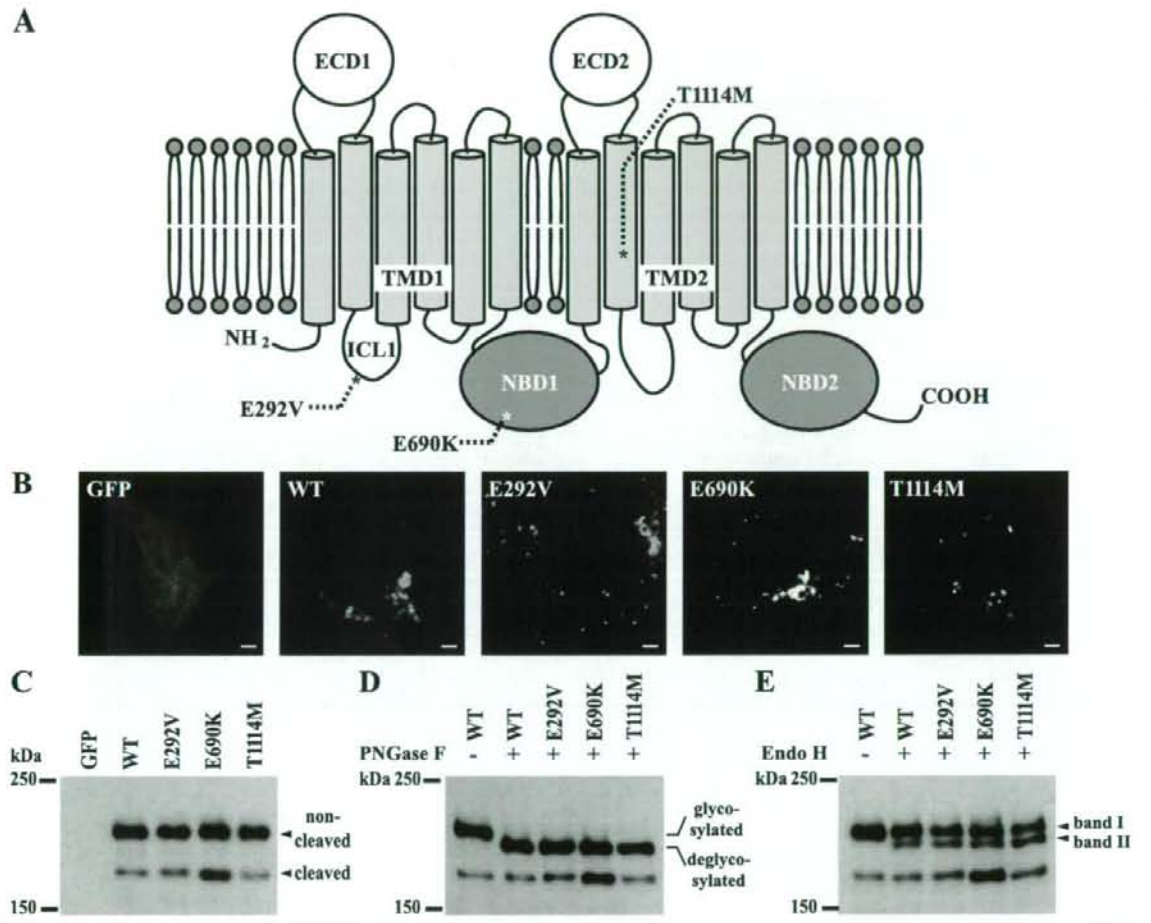

Fig. 1. Structural model of ATP-binding cassette transporter ABCA3 protein and intracellular localization and glycosylation of wild-type ABCA3-green fluorescent protein (GFP) and pediatric interstitial lung disease (pILD) mutant proteins. *A*: locations of pILD mutations characterized in this study are indicated. ABCA3 is constituted by 2 transmembrane domains (TMD), each of which contains 6 putative transmembrane segments (TM), 2 extracellular domains (ECD), and 2 nucleotide binding domains (NBD). There are 3 asparagine residues (Asp53, Asp124, and Asp140) with a consensus *N*-glycosylation motif (NXS/T) in ECD1 but not in ECD2. *B*: intracellular localization of GFP, wild-type ABCA3-GFP protein (WT), and its mutants (E292V, E690K, and T1114M) transiently expressed in human embryonic kidney HEK-293 cells were determined by confocal microscopy. Scale bar, 2 μm. *C*: total membrane fractions from HEK-293 cells transiently transfected with GFP, WT ABCA3-GFP, or mutants were subjected to SDS-PAGE, transferred to polyvinylidene difluoride (PVDF) membranes, and analyzed using anti-GFP monoclonal antibody. The positions of noncleaved (220 kDa) and cleaved (180 kDa) ABCA3-GFP proteins are indicated. *D*: total membrane fraction with (+) or without (−) treatment of peptide *N*-glycosidase F (PNGase F) was subjected to SDS-PAGE and analyzed by immunoblotting. ABCA3-GFP proteins modified with oligosaccharide (220 kDa) were deglycosylated by PNGase F, producing 210-kDa proteins. *E*: total membrane fraction with or without treatment of endoglycosidase H (Endo H) was subjected to SDS-PAGE and analyzed by immunoblotting. *Band I* shows Endo H-insensitive 220-kDa ABCA3-GFP proteins containing complex-type sugar chains, whereas *band II* shows Endo H-sensitive 210-kDa proteins modified with high-mannose-type sugar chains.

ABCA3-GFP protein (Fig. 1*D*). In the E292V, E690K, and T1114M mutant proteins, 50–60% of the 220-kDa protein remained as Endo H-insensitive complex-type protein (Fig. 1*E*), indicating that intracellular trafficking and processing of oligosaccharide of these mutant proteins are largely preserved and that these mutations are not type I mutations.

Lipid transport function of ABCA3-GFP and pILD mutant proteins. The lipid transport function of ABCA3 protein has been investigated using non-lung HEK-293 cells or lung adenocarcinoma A549 cells transfected with ABCA3 (7, 18). In this study, we established HEK-293 cells stably expressing pILD mutant ABCA3-GFP proteins that can be used to analyze both lipid transport function and nucleotide trapping of ABCA3 proteins. ABCA3 mediates uptake of choline-phospholipids into LAMP3-positive vesicles to convert lysosomal organelles into lamellar body-like organelles (7, 18). The lipid transport function of ABCA3 protein can therefore be evaluated by comparing endogenous content of choline-phospholipid-rich vesicles and the level of LAMP3, a marker of lysosomal organelles such as multivesicular bodies and lamellar bodies (34, 35). Expression of wild-type ABCA3-GFP in HEK-293 cells was found to increase the level of LAMP3, as well as the

choline-phospholipid level and low-density and choline-phospholipid-rich vesicle contents (Fig. 2, *A*, *B*, and *D*), as we previously found in A549 cells (18). Immunoblot analysis using anti-GFP antibody revealed that three mutant ABCA3-GFP proteins were expressed at a level similar to that in wild-type protein (Fig. 2*A*). The level of LAMP3 in E292V transfectant was comparable to that in wild-type transfectant, whereas those in E690K and T1114M transfectants were lower than in wild-type transfectant (Fig. 2*A* and Supplemental Fig. 1*A*). (Supplemental data for this article is available online at the *American Journal of Physiology-Lung Cellular and Molecular Physiology* website.) The smeared appearance of the immunoblot signal reflects high glycosylation states of LAMP3 protein (16). On the other hand, the levels of GRP78, a marker of endoplasmic reticulum, were similar in the five cell lines. These results indicate that expression of pILD mutant ABCA3-GFP proteins affects lysosomal organelles in differing degrees.

To investigate the effect of ABCA3 expression on the endogenous lipid level, we analyzed the contents of choline-phospholipids and total cholesterol in these cell lines. The levels of choline-phospholipids were significantly increased 1.38- and 1.13-fold in wild-type and E292V transfectants, respectively, compared with the level in HEK-293 cells, whereas levels in E690K and T1114M transfectants were similar to that in HEK-293 cells (Fig. 2*B*). On the other hand, the levels of total cholesterol were similar in the five cell lines (Fig. 2*C*).

We then investigated sucrose gradient fractionation to identify low-density and choline-phospholipid-rich vesicle formation in mutant transfectants. In this gradient system, choline-phospholipid-rich vesicles generated by ABCA3-mediated lipid transport migrate to the lower fractions in a manner similar to lamellar bodies from native lung tissue (18). In wild-type transfectant, endogenous choline-phospholipid content in the lower fractions (*fractions 2–4*) was higher than in HEK-293 cells (Fig. 2*D*). In addition, in wild-type transfectant, LAMP3 was detected mainly in *fractions 2–4* and *10*, whereas LAMP3 was detected mainly in *fraction 10* and partly in *fractions 4–6* in HEK-293 cells (Supplemental Fig. 1*B*). Thus the increased choline-phospholipid content in the lower fractions and the shift of LAMP3 distribution into lower fractions reflect ABCA3-mediated uptake of choline-phospholipids into LAMP3-positive vesicles to convert lysosomal organelles into lower density and lipid-rich vesicles (7, 18). In E292V transfectant, choline-phospholipid content in *fractions 2–4* was higher than that in HEK-293 cells and lower than that in wild-type transfectant. In E690K transfectant, the distribution of choline-phospholipid content was similar to that in HEK-293 cells. In T1114M transfectant, choline-phospholipid content in *fractions 2–4* was somewhat higher than that in HEK-293 cells, but the difference was not statistically significant ($n = 4$, Supplemental Fig. 1*C*). Considered together, these results suggest that although the lipid transport function of the E292V mutant protein is moderate, those of the E690K and T1114M mutant proteins are severely impaired.

Abnormalities of ATP binding and/or hydrolysis in pILD mutant proteins. To clarify the mechanism of impaired lipid transport in the pILD mutant proteins, we compared ATP

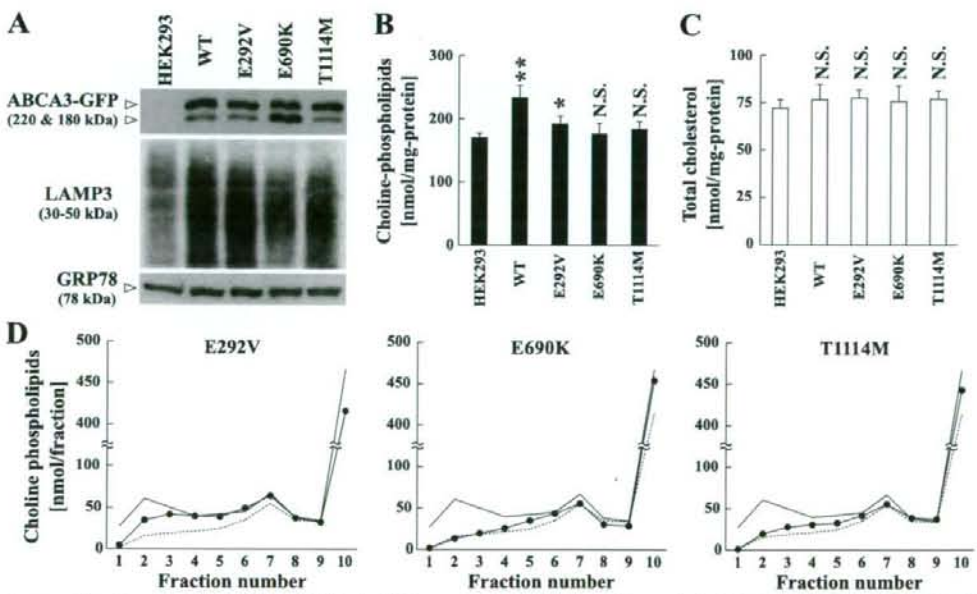

Fig. 2. Lipids transport function of wild-type ABCA3-GFP and pILD mutant proteins. *A*: Immunoblot analysis of the level of ABCA3-GFP, LAMP3, and GRP78 in HEK-293 cells stably expressing WT ABCA3-GFP, E292V, E690K, T1114M, or untransfected HEK-293 cells. *B* and *C*: the contents of endogenous choline-phospholipids (*B*) and total cholesterol (*C*) in postnuclear supernatant (PNS) of each cell type. Data are means ± SD ($n = 6–9$). *$P < 0.05$; **$P < 0.01$ vs. HEK-293 cells. N.S., not significant. *D*: sucrose gradient fractionation of intracellular compartments from each cell type. PNS (4 mg of protein) was fractionated in a sucrose gradient. *Fractions 1* and *10* are the lowest and highest density fractions, respectively. The contents of endogenous choline-phospholipids are shown. For comparison, the lipid content of HEK-293 cells stably expressing wild-type ABCA3 (solid line) and untransfected HEK-293 cells (broken line) are shown. Experiments were performed 4 times, and representative data are shown.

hydrolysis of these mutants by using a vanadate-induced nucleotide trapping technique (28, 32). ABCA3 protein efficiently traps Mg-ADP in the presence of orthovanadate, an analog of phosphate, and forms a stable inhibitory intermediate during the ATP hydrolysis cycle (17, 21). This intermediate can be specifically photoaffinity labeled in the membrane after ATP hydrolysis when 8-azido-[α-^{32}P]ATP is used as an ATP analog, allowing assessment of ATP hydrolysis with production of a stable intermediate based on the intensity of photoaffinity labeling.

As previously reported (17), among 20,000-*g* membrane fractions of cells expressing wild-type ABCA3-GFP, 220-kDa (noncleaved form) and 180-kDa (cleaved form) proteins were slightly photoaffinity labeled with 8-azido-[α-^{32}P]ATP in the absence of orthovanadate (Fig. 3*A*, *lane 3*), and photoaffinity labeling was further induced in the presence of orthovanadate (Fig. 3*A*, *lane 4*). In vanadate-induced nucleotide trapping by the E292V and T1114M mutant proteins, ATP hydrolysis with production of a photoaffinity-labeled intermediate was decreased to 40 and 52% of that of wild-type protein, respectively (Fig. 3*A*, *lanes 5*, *6*, *9*, and *10*, and *B*). On the other hand, in the E690K mutant protein, it was increased to 200% of that of wild-type protein (Fig. 3*A*, *lanes 7* and *8*, and *B*).

To investigate the altered ATP hydrolysis with production of a photoaffinity-labeled intermediate in the mutant proteins, we examined ATP binding of ABCA3-GFP proteins by photoaffinity labeling with 8-azido-[γ-^{32}P]ATP at 0°C. In this nonhydrolytic condition, ABCA3-GFP proteins are labeled only with nucleotides before hydrolysis, allowing determination of ATP binding based on the intensity of photoaffinity labeling. Among the 20,000-*g* membrane fractions of cells expressing wild-type ABCA3-GFP, 220- and 180-kDa proteins were photoaffinity labeled with 8-azido-[γ-^{32}P]ATP, whereas membrane fractions of untransfected cells were not photoaffinity labeled (Fig. 3*C*). ATP binding of the E292V and T1114M mutant proteins determined by photoaffinity labeling with 8-azido-[γ-^{32}P]ATP was similar to that of wild-type ABCA3-GFP protein (Fig. 3, *C* and *D*). However, in E690K mutant protein, photoaffinity labeling of the 220-kDa protein was similar to that of wild type protein regardless of decreased noncleaved form protein, and photoaffinity labeling of the 180-kDa protein was dramatically enhanced even when the increased levels of the cleaved form of the protein were taken into consideration. When normalized to the level of ABCA3-GFP proteins (total 220-kDa noncleaved form plus 180-kDa cleaved form), photoaffinity labeling of the E690K mutant protein was increased to 250% of that of wild-type protein. These results show that the catalytic cycles of these mutant proteins differ from that of wild-type protein and that these mutations in pILD are type II mutations.

Mutational analysis of Glu292 in ICL-1 and Thr1114 in putative TM-8. To investigate the mechanism of loss of ATP hydrolysis with production of a photoaffinity-labeled intermediate in E292V and T1114M mutant proteins, we performed mutational analyses of Glu292 residue in ICL-1 and Thr1114 in putative TM-8. The Glu or Asp residue in ICL-1 is conserved in members of the ABCA subfamily (Fig. 4*A*), suggesting the importance of negatively charged amino acids in ICL-1 for ATP hydrolysis. To clarify this, we substituted Glu292 with Asp and Lys, which are negatively and positively charged, respectively. In vanadate-induced nucleotide trapping by E292D mutant protein, production of a photoaffinity-labeled

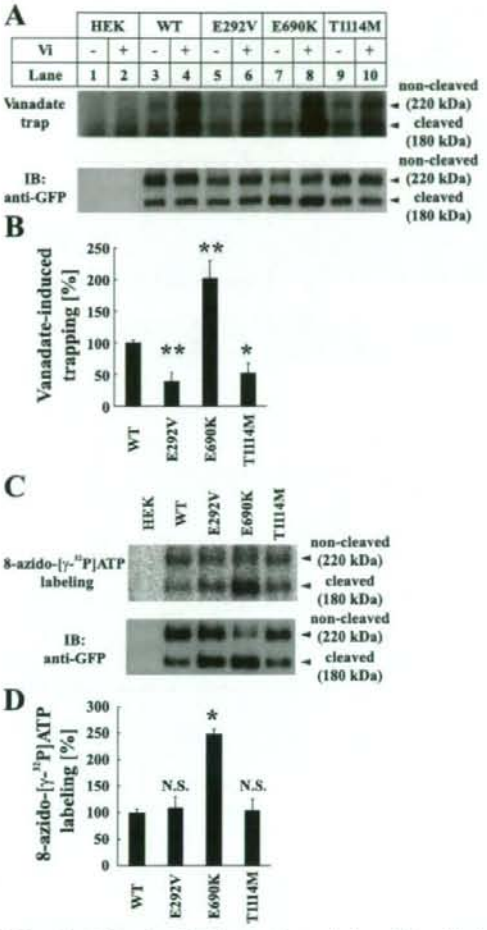

Fig. 3. Vanadate-induced nucleotide trapping and photoaffinity labeling of ABCA3-GFP and pILD mutant proteins using 8-azido-[^{32}P]ATP. *A*: 20,000-*g* membrane fraction prepared from HEK-293 cells stably expressing the WT ABCA3-GFP (*lanes 3* and *4*), E292V (*lanes 5* and *6*), E690K (*lanes 7* and *8*), T1114M (*lanes 9* and *10*), or untransfected HEK-293 cells (*lanes 1* and *2*) was incubated with 10 μM 8-azido-[α-^{32}P]ATP in the absence (−) or presence (+) of 0.4 mM orthovanadate (Vi) and 3 mM $MgCl_2$ for 10 min at 37°C. Protein was photoaffinity labeled with UV irradiation after removal of unbound ATP, electrophoresed on SDS-PAGE, and transferred to a PVDF membrane. Membrane was analyzed by autoradiography (*top*) and immunoblotting (IB) using anti-GFP antibody (*bottom*). *B*: radioactivity of photoaffinity-labeled protein (total 220-kDa noncleaved form plus 180-kDa cleaved form) was quantified by FLA-5000. Radioactivity in the absence of orthovanadate was subtracted from that in the presence of orthovanadate and is expressed after normalization to the level of ABCA3-GFP protein (total 220-kDa noncleaved form plus 180-kDa cleaved form). Data are means ± SD (n = 4). *$P < 0.05$; **$P < 0.01$ vs. WT. *C*: 20,000-*g* membrane fraction prepared from HEK-293 cells stably expressing the WT ABCA3-GFP, E292V, E690K, T1114M, or untransfected HEK-293 cells was incubated with 40 μM 8-azido-[γ-^{32}P] and 3 mM $MgCl_2$ for 10 min at 0°C. Protein was photoaffinity labeled with UV irradiation, immunoprecipitated with anti-human ABCA3 antibody, electrophoresed on SDS-PAGE, and transferred to a PVDF membrane. Membrane was analyzed by FLA-5000 (*top*) and IB using anti-GFP antibody (*bottom*). *D*: radioactivity of photoaffinity-labeled protein (total 220-kDa noncleaved form plus 180-kDa cleaved form) was quantified by FLA-5000 and is expressed after normalization to the level of ABCA3-GFP protein (total 220-kDa noncleaved form plus 180-kDa cleaved form). Data are means ± SD (n = 3). *$P < 0.01$ vs. WT.

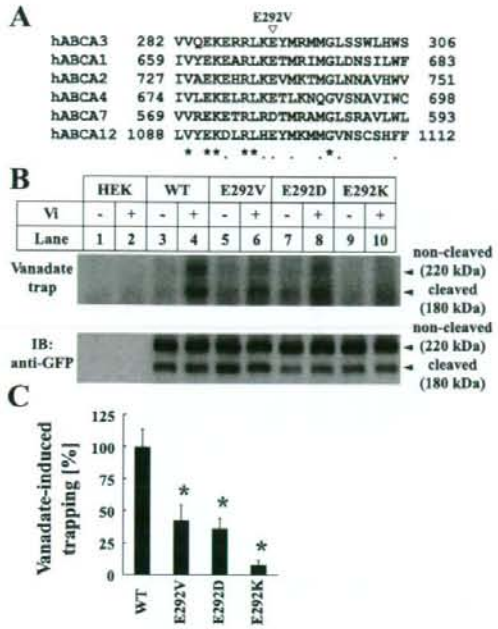

Fig. 4. Alignment of amino acid sequence of intracellular loop 1 (ICL-1) and vanadate-induced nucleotide trapping in site-directed mutant proteins of Glu292. *A*: alignment of amino acid sequence of ICL-1 of some members of the human ABCA subfamily is shown. The amino acid residues that are conserved in 6 transporters and in 4 or 5 transporters are indicated by asterisks and dots, respectively. *B*: 20,000-*g* membrane fraction prepared from HEK-293 cells stably expressing the WT ABCA3-GFP (*lanes 3* and *4*), E292V (*lanes 5* and *6*), E292D (*lanes 7* and *8*), E292K (*lanes 9* and *10*), or untransfected HEK-293 cells (*lanes 1* and *2*) was incubated with 10 μM 8-azido-[α-^{32}P]ATP in the absence or presence of 0.4 mM Vi and 3 mM $MgCl_2$ for 10 min at 37°C. Protein was photoaffinity labeled with UV irradiation after removal of unbound ATP, electrophoresed on SDS-PAGE, and transferred to a PVDF membrane. Membrane was analyzed by autoradiography (*top*) and IB using anti-GFP antibody (*bottom*). *C*: radioactivity of photoaffinity-labeled protein (total 220-kDa noncleaved form plus 180-kDa cleaved form) was quantified by FLA-5000. Radioactivity in the absence of orthovanadate was subtracted from that in the presence of orthovanadate and is expressed after normalization to the level of ABCA3-GFP protein (total 220-kDa noncleaved form plus 180-kDa cleaved form). Data are means ± SD (n = 3). *P < 0.01 vs. WT.

intermediate during ATP hydrolysis was decreased to 37% of that of wild-type protein, as also was the case in E292V mutant protein (Fig. 4*B*, *lanes 5–8*, and *C*). In E292K mutant protein, it was decreased to 4% of that of wild-type protein (Fig. 4*B*, *lanes 9* and *10*, and *C*). These results indicate that not only a negative charge but also an appropriate side chain length of Glu292 at ICL-1 is important for production of a photoaffinity-labeled intermediate during ATP hydrolysis of ABCA3 protein.

Recently, we identified a novel compound heterozygous mutation (maternal T1114A and paternal W1148X) from a Japanese boy with respiratory distress from age 18 mo (37). The T1114A mutation decreased vanadate-induced nucleotide trapping by ABCA3 protein similarly to the T1114M mutation. Because ABCA1, ABCA2, ABCA4, ABCA7, and ABCA12 have conserved Ser residues rather than a Thr residue in putative TM-8 (Fig. 5*A*), loss of the hydroxyl group-containing amino acid might well act on putative TM-8 to hamper communication between transmembrane domains (TMDs) and NBDs, resulting in loss of ATP hydrolysis activity. To clarify this, we substituted Thr1114 with Ser and examined vanadate-induced nucleotide trapping. In vanadate-induced nucleotide trapping by T1114S mutant protein, production of a photoaffinity-labeled intermediate during ATP hydrolysis was found to be similar to that of wild-type protein, whereas that of T1114M and T1114A mutant protein was 56 and 47% of wild-type protein, respectively (Fig. 5*B*, *lanes 5–10*, and *C*). These results indicate that loss of the hydroxyl group of the 1114th amino acid is responsible for the impaired ATP hydrolysis with production of a photoaffinity-labeled intermediate in both the T1114M and T1114A mutant proteins.

Interaction of E690K mutant ABCA3-GFP protein with nucleotides. To investigate the mechanism of enhanced production of a photoaffinity-labeled intermediate during ATP hydrolysis in E690K mutant protein, we performed the trap-

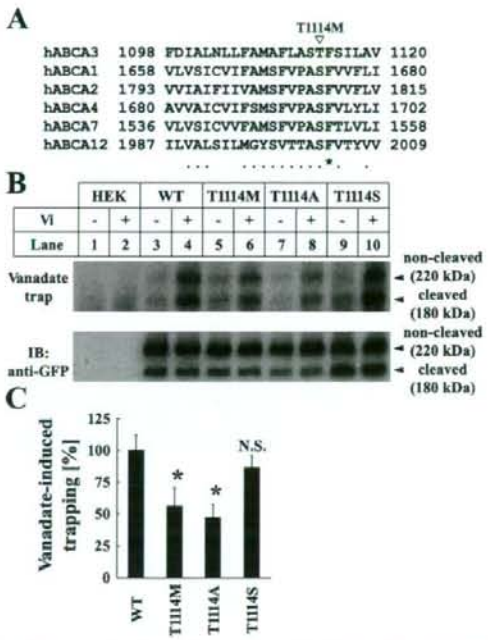

Fig. 5. Alignment of amino acid sequence of the 8th putative transmembrane segment (TM-8) and vanadate-induced nucleotide trapping in site-directed mutant proteins of Thr1114. *A*: alignment of amino acid sequence of putative TM-8 of some members of the human ABCA subfamily is shown. The amino acids residues that are conserved in 6 transporters and in 4 or 5 transporters are indicated by asterisks and dots, respectively. *B*: 20,000-*g* membrane fraction prepared from HEK-293 cells stably expressing the WT ABCA3-GFP (*lanes 3* and *4*), T1114M (*lanes 5* and *6*), T1114A (*lanes 7* and *8*), T1114S (*lanes 9* and *10*), or untransfected HEK-293 cells (*lanes 1* and *2*) was incubated with 10 μM 8-azido-[α-^{32}P]ATP in the absence or presence of 0.4 mM Vi and 3 mM $MgCl_2$ for 10 min at 37°C. Proteins were photoaffinity labeled with UV irradiation after removal of unbound ATP, electrophoresed on SDS-PAGE, and transferred to a PVDF membrane. Membrane was analyzed by autoradiography (*top*) and IB using anti-GFP antibody (*bottom*). *C*: radioactivity of photoaffinity-labeled protein (total 220-kDa noncleaved form plus 180-kDa cleaved form) was quantified by FLA-5000. Radioactivity in the absence of orthovanadate was subtracted from that in the presence of orthovanadate and is expressed after normalization to the level of ABCA3-GFP protein (total 220-kDa noncleaved form plus 180-kDa cleaved form). Data are means ± SD (n = 3). *P < 0.01 vs. WT.

ping experiments using 8-azido-[γ-^{32}P]ATP. In this procedure, a posthydrolyzed trapped nucleotide should not be detected by vanadate-induced trapping because of hydrolytic loss of [γ-^{32}P]PO_4. Indeed, in the presence of orthovanadate, photoaffinity labeling of wild-type and E690K mutant proteins with 8-azido-[γ-^{32}P]ATP was barely detectable (Fig. 6*A*). These data combined with vanadate-induced trapping using 8-azido-[α-^{32}P]ATP indicate that E690K mutant protein hydrolyzes 8-azido-[α-^{32}P]ATP and releases γ-phosphate and that the nucleotide trapped by E690K mutant protein is mostly in the ADP form.

In E690K mutant protein, ATP binding determined by photoaffinity labeling with 8-azido-[γ-^{32}P]ATP was dramatically increased compared with that of wild-type protein (see Fig. 3, *C* and *D*). To determine whether the E690K mutation alters ADP binding, we performed labeling experiments using 8-azido-[α-^{32}P]ADP at 0°C. In this condition, photoaffinity labeling of E690K mutant protein was comparable to that of wild-type ABCA3-GFP protein (Fig. 6, *B* and *C*), suggesting that γ-phosphate of 8-azido-[γ-^{32}P]ATP contributes to enhanced photoaffinity labeling in E690K mutant protein.

Since some mutations in the Glu residues following the Walker B motif have been reported to interfere with the ATP-hydrolysis cycle including the ADP release step (5, 24, 25, 33), we examined release of trapped nucleotides from wild-type and E690K mutant ABCA3-GFP proteins. A 20,000-*g* membrane fraction was first incubated for 10 min at 37°C with 8-azido-[α-^{32}P]ATP in the presence of orthovanadate, and unbound nucleotides were removed by washing. The membrane fraction was reincubated at 37°C for 0–15 min in buffer containing $MgCl_2$ before cross-linking. In wild-type ABCA3-GFP protein, trapped nucleotides were time-dependently reduced by reincubation, and photoaffinity labeling at 5 min was 32% of that at 0 min (Fig. 6, *D* and *E*). In contrast, in E690K mutant protein, trapped nucleotides were more slowly released than in wild-type protein, and photoaffinity labeling at 5 min was 73% of that at 0 min, suggesting that E690K mutant protein forms a more stable inhibitory intermediate after hydrolysis of 8-azido-[α-^{32}P]ATP than wild-type protein. Thus these data further suggest abnormal interaction with nucleotides in E690K mutant protein.

Mutational analysis of Glu690 adjacent to walker B motif in NBD-1. To further clarify the enhanced production of a photoaffinity-labeled intermediate during ATP hydrolysis in E690K mutant, we performed mutational analyses of the Glu690 residue adjacent to the Walker B motif in NBD-1. Because Glu and Lys are negatively and positively charged amino acids, respectively, alteration of charge at the 690th amino acid residue could well be responsible for the abnormal interaction with nucleotides in the E690K mutant. Accordingly, Glu690 was substituted with Asp and Arg, which are negatively and positively charged, respectively. Substitution with Asp and Arg caused a dramatic

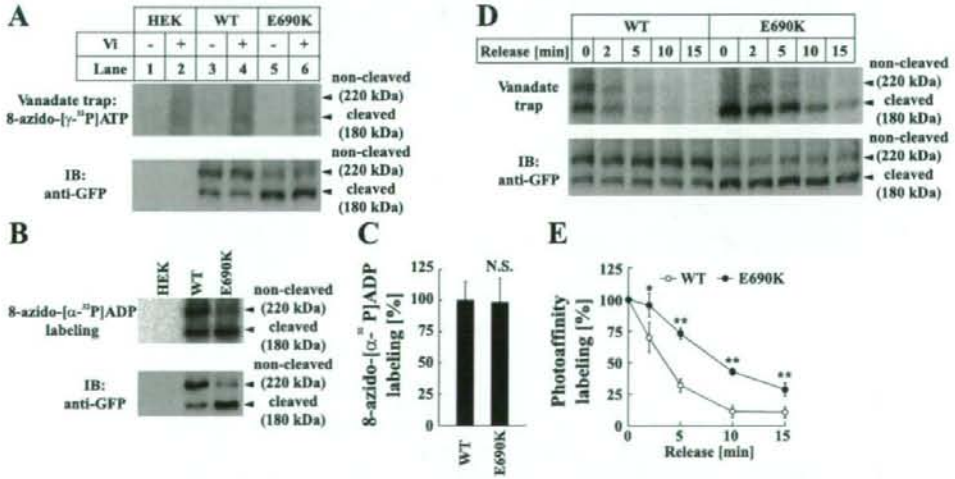

Fig. 6. Interaction of E690K mutant ABCA3-GFP protein with nucleotides. *A*: 20,000-*g* membrane fraction prepared from HEK-293 cells stably expressing the WT ABCA3-GFP (*lanes 3* and *4*) E690K (*lanes 5* and *6*), or untransfected HEK-293 cells (*lanes 1* and *2*) was incubated with 10 μM 8-azido-[γ-^{32}P] ATP in the absence or presence of 0.4 mM Vi and 3 mM $MgCl_2$ for 10 min at 37°C. Protein was photoaffinity labeled with UV irradiation after removal of unbound ATP, electrophoresed on SDS-PAGE, and transferred to a PVDF membrane. Membrane was analyzed by autoradiography (*top*) and IB using anti-GFP antibody (*bottom*). *B*: 20,000-*g* membrane fraction prepared from HEK-293 cells stably expressing the WT ABCA3-GFP, E690K, or untransfected HEK-293 cells was incubated with 40 μM 8-azido-[α-^{32}P]ADP and 3 mM $MgCl_2$ for 10 min at 0°C. Protein was photoaffinity labeled with UV irradiation, immunoprecipitated with anti-human ABCA3 antibody, electrophoresed on SDS-PAGE, and transferred to a PVDF membrane. Membrane was analyzed by FLA-5000 (*top*) and IB using anti-GFP antibody (*bottom*). *C*: radioactivity of photoaffinity-labeled protein (total 220-kDa noncleaved form plus 180-kDa cleaved form) was quantified by FLA-5000 and is expressed after normalization to the level of ABCA3-GFP protein (total 220-kDa noncleaved form plus 180-kDa cleaved form). Data are means ± SD (n = 3). *D*: 20,000-*g* membrane fraction prepared from HEK-293 cells stably expressing the WT ABCA3-GFP or E690K was first incubated for 10 min at 37°C with 10 μM 8-azido-[α-^{32}P]ATP in the presence of orthovanadate, and unbound nucleotides were removed by washing. A membrane fraction was reincubated at 37°C for 0–15 min in a buffer containing $MgCl_2$, before cross-linking. After removal of released nucleotides and cross-linking, protein was electrophoresed on SDS-PAGE and transferred to a PVDF membrane. Membrane was analyzed by autoradiography (*top*) and IB using anti-GFP antibody (*bottom*). *E*: radioactivity of photoaffinity-labeled protein (total 220-kDa noncleaved form plus 180-kDa cleaved form) was quantified by FLA-5000 and is expressed as a percentage of the 0-min value after normalization to the level of ABCA3-GFP protein (total 220-kDa noncleaved form plus 180-kDa cleaved form). Data are means ± SD (n = 4). *$P < 0.05$; **$P < 0.01$ vs. WT.

decrease in ATP hydrolysis with production of a photoaffinity-labeled intermediate to 11 and 12% of that of wild-type protein, respectively (Fig. 7, *A* and *B*). These results show that both negative charge and side chain length of Glu690 are important for ATP hydrolysis of wild-type ABCA3 protein and that not only positive charge but also side chain length of Lys690 contribute to enhanced production of a photoaffinity-labeled intermediate during ATP hydrolysis in the E690K mutant protein.

DISCUSSION

In the present study, to clarify the phenotypic heterogeneity of lung disease associated with *ABCA3* mutation, we characterized the ABCA3 mutant proteins identified in pILD patients, a more mild disease than fatal surfactant deficiency. Although E292V, E690K, and T1114M mutant proteins were found to traffic to intracellular vesicles, the lipid transport function of E292V mutant protein was partially impaired, and those of E690K and T1114M mutant protein were severely impaired, accompanied by an aberrant catalytic cycle. We recently found that fatal surfactant deficiency due to *ABCA3* mutation comprises defects of abnormal intracellular localization (type I) and normal intracellular localization with decreased ATP hydrolysis of ABCA3 protein (type II) (17). Accordingly, E292V, E690K, and T1114M are type II mutations.

Patients with fatal surfactant deficiency carrying a type I homozygous *ABCA3* mutation (W1142X/W1142X, L101P/L101P, or L1553P/L1553P) or a type I/type II compound heterozygous mutation (L982P/G1221S or Ins1518/L1580P) die within the neonatal period (Table 1) (27). On the other hand, patients carrying a type II/type II *ABCA3* mutation (E292V/T1114M or E292V/E690K) exhibit pILD (4), suggesting that the type II/type II *ABCA3* mutation produces a milder phenotype. Although an exception has been identified in a Japanese patient with a type I/type II *ABCA3* mutation (W1148X/T1114A) (37), the moderately preserved lipid transport function of the E292V mutant protein may underlie the generally milder phenotype of pILD patients. Further analysis using transgenic mice is required to understand the impacts of these mutations on surfactant metabolism in vivo.

Table 1. *Genotype-phenotype correlation for ABCA3 mutation*

ABCA3 Mutation		Age of Symptoms	Phenotype	Ref.
W1142X	*W1142X*	Neonate	FSD	27
L101P	*L101P*	Neonate	FSD	27
L1553P	*L1553P*	Neonate	FSD	27
Ins1518	L1580P	Neonate	FSD	27
L982P	G1221S	Neonate	FSD	27
E292V	T1114M	Neonate	pILD	4
E292V	E690K	5 or 7 yr	pILD	4
W1148X	T1114A	12 mo	pILD	37

Type I and type II ATP binding cassette A3 (*ABCA3*) mutations are shown in italics and roman, respectively. FSD, fatal surfactant deficiency; Ins1518, Ins1518fs/ter1519; pILD, pediatric interstitial lung disease.

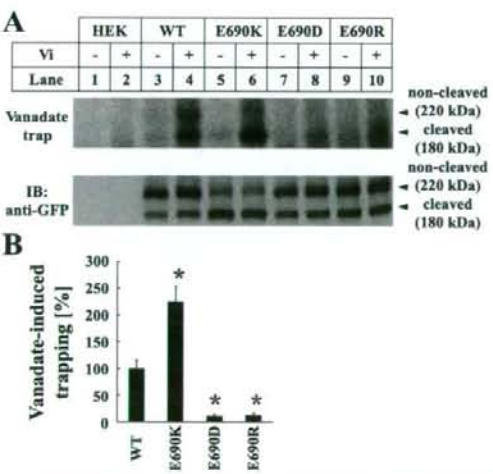

Fig. 7. Vanadate-induced nucleotide trapping in site-directed mutant proteins of Glu690. *A*: 20,000-*g* membrane fraction prepared from HEK-293 cells stably expressing the WT ABCA3-GFP (*lanes 3* and *4*), E690K (*lanes 5* and *6*), E690D (*lanes 7* and *8*), E690R (*lanes 9* and *10*), or untransfected HEK-293 cells (*lanes 1* and *2*) was incubated with 10 μM 8-azido-[α-^{32}P]ATP in the absence or presence of 0.4 mM Vi and 3 mM $MgCl_2$ for 10 min at 37°C. Protein was photoaffinity labeled with UV irradiation after removal of unbound ATP, electrophoresed on SDS-PAGE, and transferred to a PVDF membrane. Membrane was analyzed by autoradiography (*top*) and IB using anti-GFP antibody (*bottom*). *B*: radioactivity of photoaffinity-labeled protein (total 220-kDa noncleaved form plus 180-kDa cleaved form) was quantified by FLA-5000. Radioactivity in the absence of orthovanadate was subtracted from that in the presence of orthovanadate and is expressed after normalization to the level of ABCA3-GFP protein (total 220-kDa noncleaved form plus 180-kDa cleaved form). Data are means ± SD (n = 3). *P < 0.01 vs. WT.

The E292V mutant protein exhibits moderately preserved lipid transport function and vanadate-induced nucleotide trapping, and mutational analysis of Glu292 in ICL-1 indicates the significance of both negative charge and side chain length of Glu292 for ATP hydrolysis with production of a photoaffinity-labeled intermediate in ABCA3 protein. In addition, the recently solved crystal structure of the bacterial ABC transporter Sav1866 suggests that ICLs interact with NBDs and TMDs to transmit conformational changes generated by ATP binding and hydrolysis from NBDs to TMDs (9). Thus the E292V mutation might impede the transmission of conformational changes, resulting in moderate impairment of lipid transport in ABCA3 protein.

The T1114M mutant protein exhibits impaired lipid transport function accompanied by moderately preserved vanadate-induced nucleotide trapping. In addition, mutational analysis of Thr1114 in putative TM-8 shows the importance of the hydroxyl group of the 1114th amino acid residue for ATP hydrolysis with production of a photoaffinity-labeled intermediate in ABCA3 protein. In membrane proteins, the hydroxyl group of Ser and that of Thr are known to form a hydrogen bond with backbone nitrogen to contribute to tight helix packing (10), suggesting that loss of the hydroxyl group from the 1114th amino acid in putative TM-8 might well hamper conformational change of TMDs during ATP-hydrolysis that results in impaired lipid transport of the ABCA3 protein.

The glutamate residue following the Walker B motif in ABC transporters has been suggested to be a catalytic carboxylate that facilitates nucleophilic attack on ATP via a water molecule (13, 23). However, it has been reported that some mutations in the Glu residues interfere with ADP release (5, 24, 25, 33) and tight dimerization of NBDs (29, 30, 31). In E690K mutant

ABCA3 protein, lipid transport function is severely impaired, accompanied by abnormal interaction with nucleotides: enhanced vanadate-induced nucleotide trapping at 37°C, enhanced photoaffinity labeling with 8-azido-[γ-^{32}P]ATP at 0°C, and delayed release of 8-azido-[α-^{32}P]ADP after vanadate-induced nucleotide trapping. Furthermore, mutational analysis of Glu690 indicates that side chain length of Lys690 contributes to enhanced production of a photoaffinity-labeled intermediate during ATP hydrolysis in the E690K mutant protein. To clarify the origin of the abnormal interaction with nucleotides in E690K mutant protein, we modeled the structure of NBD-1 of ABCA3 based on the crystal structure of *E. coli* MalK using SWISS-MODEL (Supplemental Fig. 2). In the wild-type ABCA3 model, the distance from side chain oxygen of Glu690 to γ-phosphate oxygen of ATP is ~7.1 Å, similar to the distance from side chain oxygen of Glu159 in MalK. On the other hand, in the model of E690K mutant, the distance from side chain nitrogen of Lys690 to γ-phosphate oxygen of ATP is ~3.6 Å. One possible interpretation of these biochemical results and modeling is that ionic interaction of Lys690 and γ-phosphate of ATP in the E690K mutant protein may tighten the binding of ATP in NBD-1, resulting in delayed ADP release after ATP hydrolysis, probably in NBD-2. Another possible interpretation is that the interaction of Lys690 with γ-phosphate of ATP may alter the directionality of the adenine moiety of ATP, increasing the efficiency of photoaffinity labeling with 8-azido-ATP. Analysis using purified ABCA3 protein would further clarify the aberrant catalytic cycle and impaired lipid transport in E690K mutant protein.

The cleaved form of ABCA3 protein is predominantly expressed in native lung tissue (11, 18, 36) and shows increased vanadate-induced trapping compared with the noncleaved form of the protein in HEK-293 cells. Furthermore, cleavage of ABCA3 protein at ECD1 is suggested to be important for fully active transport function (unpublished observation). Since the cleaved form was rarely detected in ABCA3 mutant protein that remained localized to endoplasmic reticulum (17), the cleavage of ABCA3 protein may occur in Golgi or post-Golgi compartments. Interestingly, in E690K mutant protein, the amount of 180-kDa cleaved form was increased compared with that of wild-type protein. The increased level of 180-kDa cleaved form E690K mutant protein might be due to the abnormal nucleotide-bound conformation of E690K mutant protein being preferentially cleaved by enzymes within intracellular vesicles, compared with that in wild-type protein. Further studies to determine cleavage sites and the enzymes involved in the cleavage of ABCA3 protein are needed.

In summary, the moderately preserved lipid transport function of E292V mutant protein may be responsible for the milder phenotype in pILD caused by *ABCA3* mutation compared with that in fatal surfactant deficiency. The molecular mechanisms of the impaired lipid transport function of ABCA3 could be key to developing treatment strategies to restore ABCA3 function in patients with *ABCA3* mutation.

ACKNOWLEDGMENTS

We thank Drs. Jun-ichi Miyazaki (Osaka University) and Hitoshi Niwa (RIKEN, Kobe) for providing the pCAGIpuro plasmid.

Present address of Y. Matsumura: Dept. of Biochemistry and Molecular Biology, Oregon Health and Science Univ., Portland, OR 97239.

GRANTS

This work was supported by Scientific Research Grants and Grant-in-Aid for Creative Scientific Research 15GS0301 from the Ministry of Education, Culture, Sports, Science and Technology of Japan; Core Research for Evolutional Science and Technology of Japan Science and Technology Agency; the 21st Century Center of Excellence Program; and the Manpei Suzuki Diabetes Foundation.

REFERENCES

1. **Ban N, Matsumura Y, Sakai H, Takanezawa Y, Sasaki M, Arai H, Inagaki N.** ABCA3 as a lipid transporter in pulmonary surfactant biogenesis. *J Biol Chem* 282: 9628–9634, 2007.
2. **Bligh EG, Dyer WJ.** A rapid method of total lipid extraction and purification. *Can J Biochem Physiol* 37: 911–917, 1959.
3. **Brasch F, Schimanski S, Muhlfeld C, Barlage S, Langmann T, Aslanidis C, Boettcher A, Dada A, Schroten H, Mildenberger E, Prueter E, Ballmann M, Ochs M, Johnen G, Griese M, Schmitz G.** Alteration of the pulmonary surfactant system in full-term infants with hereditary ABCA3 deficiency. *Am J Respir Crit Care Med* 174: 571–580, 2006.
4. **Bullard JE, Wert SE, Whitsett JA, Dean M, Nogee LM.** *ABCA3* mutations associated with pediatric interstitial lung disease. *Am J Respir Crit Care Med* 172: 1026–1031, 2005.
5. **Carrier I, Julien M, Gros P.** Analysis of catalytic carboxylate mutants E552Q and E1197Q suggests asymmetric ATP hydrolysis by the two nucleotide-binding domains of P-glycoprotein. *Biochemistry* 42: 12875–12885, 2003.
6. **Chen J, Lu G, Lin J, Davidson AL, Quiocho FA.** A tweezers-like motion of the ATP-binding cassette dimer in an ABC transport cycle. *Mol Cell* 12: 651–661, 2003.
7. **Cheong N, Madesh M, Gonzales LW, Zhao M, Yu K, Ballard PL, Shuman H.** Functional and trafficking defects in ATP binding cassette A3 mutants associated with respiratory distress syndrome. *J Biol Chem* 281: 9791–9800, 2006.
8. **Cheong N, Zhang H, Muniswamy M, Zhao M, Yu K, Dodia C, Fisher AB, Savani RC, Shuman H.** ABCA3 is critical for lamellar body biogenesis in vivo. *J Biol Chem* 282: 23811–23817, 2007.
9. **Dawson RJ, Locher KP.** Structure of a bacterial multidrug ABC transporter. *Nature* 443: 180–185, 2006.
10. **Eilers M, Shekar SC, Shieh T, Smith SO, Fleming PJ.** Internal packing of helical membrane proteins. *Proc Natl Acad Sci USA* 97: 5796–5801, 2000.
11. **Fitzgerald ML, Xavier R, Haley KJ, Welti R, Goss JL, Brown CE, Zhuang DZ, Bell SA, Lu N, McKee M, Seed B, Freeman MW.** ABCA3 inactivation in mice causes respiratory failure, loss of pulmonary surfactant, and depletion of lung phosphatidylglycerol. *J Lipid Res* 48: 621–632, 2007.
12. **Garmany TH, Moxley MA, White FV, Dean M, Hull WM, Whitsett JA, Nogee LM, Hamvas A.** Surfactant composition and function in patients with *ABCA3* mutations. *Pediatr Res* 59: 801–805, 2006.
13. **Geourjon C, Orelle C, Steinfels E, Blanchet C, Deleage G, Di Pietro A, Jault JM.** A common mechanism for ATP hydrolysis in ABC transporter and helicase superfamilies. *Trends Biochem Sci* 26: 539–544, 2001.
14. **Higgins CF.** ABC transporters: from microorganisms to man. *Annu Rev Cell Biol* 8: 67–113, 1992.
15. **Higgins D, Thompson J, Gibson T, Thompson JD, Higgins DG, Gibson TJ.** CLUSTAL W: improving the sensitivity of progressive multiple sequence alignment through sequence weighting, position-specific gap penalties and weight matrix choice. *Nucleic Acids Res* 22: 4673–4680, 1994.
16. **Kobayashi T, Beuchat MH, Chevallier J, Makino A, Mayran N, Escola JM, Lebrand C, Cosson P, Kobayashi T, Gruenberg J.** Separation and characterization of late endosomal membrane domains. *J Biol Chem* 277: 32157–32164, 2002.
17. **Matsumura Y, Ban N, Ueda K, Inagaki N.** Characterization and classification of ATP-binding cassette transporter ABCA3 mutants in fatal surfactant deficiency. *J Biol Chem* 281: 34503–34514, 2006.
18. **Matsumura Y, Sakai H, Sasaki M, Ban N, Inagaki N.** ABCA3-mediated choline-phospholipids uptake into intracellular vesicles in A549 cells. *FEBS Lett* 581: 3139–3144, 2007.
19. **McGuffin LJ, Bryson K, Jones DT.** The PSIPRED protein structure prediction server. *Bioinformatics* 16: 404–405, 2000.
20. **Mulugeta S, Gray JM, Notarfrancesco KL, Gonzales LW, Koval M, Feinstein SI, Ballard PL, Fisher AB, Shuman H.** Identification of

LBM180, a lamellar body limiting membrane protein of alveolar type II cells, as the ABC transporter protein ABCA3. *J Biol Chem* 277: 22147–22155, 2002.

21. **Nagata K, Yamamoto A, Ban N, Tanaka AR, Matsuo M, Kioka N, Inagaki N, Ueda K.** Human ABCA3, a product of a responsible gene for *abca3* for fatal surfactant deficiency in newborns, exhibits unique ATP hydrolysis activity and generates intracellular multilamellar vesicles. *Biochem Biophys Res Commun* 324: 262–268, 2004.
22. **Niwa H, Yamamura K, Miyazaki J.** Efficient selection for high-expression transfectants with a novel eukaryotic vector. *Gene* 108: 193–199, 1991.
23. **Orelle C, Dalmas O, Gros P, Di Pietro A, Jault JM.** The conserved glutamate residue adjacent to the Walker-B motif is the catalytic base for ATP hydrolysis in the ATP-binding cassette transporter BmrA. *J Biol Chem* 278: 47002–47008, 2003.
24. **Payen LF, Gao M, Westlake CJ, Cole SP, Deeley RG.** Role of carboxylate residues adjacent to the conserved core Walker B motifs in the catalytic cycle of multidrug resistance protein 1 (ABCC1). *J Biol Chem* 278: 38537–38547, 2003.
25. **Sauna ZE, Muller M, Peng XH, Ambudkar SV.** Importance of the conserved Walker B glutamate residues, 556 and 1201, for the completion of the catalytic cycle of ATP hydrolysis by human P-glycoprotein (ABCB1). *Biochemistry* 41: 13989–14000, 2002.
26. **Schwede T, Kopp J, Guex N, Peitsch MC.** SWISS-MODEL: an automated protein homology-modeling server. *Nucleic Acids Res* 31: 3381–3385, 2003.
27. **Shulenin S, Nogee LM, Annilo T, Wert SE, Whitsett JA, Dean M.** *ABCA3* gene mutations in newborns with fatal surfactant deficiency. *N Engl J Med* 350: 1296–1303, 2004.
28. **Taguchi Y, Yoshida A, Takada Y, Komano T, Ueda K.** Anti-cancer drugs and glutathione stimulate vanadate-induced trapping of nucleotide in multidrug resistance-associated protein (MRP). *FEBS Lett* 401: 11–14, 1997.
29. **Tombline G, Bartholomew LA, Urbatsch IL, Senior AE.** Combined mutation of catalytic glutamate residues in the two nucleotide binding domains of P-glycoprotein generates a conformation that binds ATP and ADP tightly. *J Biol Chem* 279: 31212–31220, 2004.
30. **Tombline G, Bartholomew LA, Tyndall GA, Gimi K, Urbatsch IL, Senior AE.** Properties of P-glycoprotein with mutations in the "catalytic carboxylate" glutamate residues. *J Biol Chem* 279: 46518–46526, 2004.
31. **Tombline G, Muharemagic A, White LB, Senior AE.** Involvement of the "occluded nucleotide conformation" of P-glycoprotein in the catalytic pathway. *Biochemistry* 44: 12879–12886, 2005.
32. **Urbatsch IL, Sankaran B, Weber J, Senior AE.** P-glycoprotein is stably inhibited by vanadate-induced trapping of nucleotide at a single catalytic site. *J Biol Chem* 270: 19383–19390, 1995.
33. **Urbatsch IL, Julien M, Carrier I, Rousseau ME, Cayrol R, Gros P.** Mutational analysis of conserved carboxylate residues in the nucleotide binding sites of P-glycoprotein. *Biochemistry* 39: 14138–14149, 2000.
34. **Voorhout WF, Veenendaal T, Haagsman HP, Weaver TE, Whitsett JA, van Golde LM, Geuze HJ.** Intracellular processing of pulmonary surfactant protein B in an endosomal/lysosomal compartment. *Am J Physiol Lung Cell Mol Physiol* 263: L479–L486, 1992.
35. **Wang WJ, Russo SJ, Mulugeta S, Beers MF.** Biosynthesis of surfactant protein C (SP-C). *J Biol Chem* 277: 19929–19937, 2002.
36. **Yamano G, Funahashi H, Kawanami O, Zhao LX, Ban N, Uchida Y, Morohoshi T, Ogawa J, Shioda S, Inagaki N.** ABCA3 is a lamellar body membrane protein in human lung alveolar type II cells. *FEBS Lett* 508: 221–225, 2001.
37. **Yokota T, Matsumura Y, Ban N, Matsubayashi T, Inagaki N.** Heterozygous *ABCA3* mutation associated with non-fatal evolution of respiratory distress. *Eur J Pediatr* 167: 691–693, 2008.
38. **Yoshida I, Ban N, Inagaki N.** Expression of ABCA3, a causative gene for fatal surfactant deficiency, is up-regulated by glucocorticoids in lung alveolar type II cells. *Biochem Biophys Res Commun* 323: 547–555, 2004.
39. **Zaitseva J, Jenewein S, Jumpertz T, Holland IB, Schmitt L.** H662 is the linchpin of ATP hydrolysis in the nucleotide-binding domain of the ABC transporter HlyB. *EMBO J* 24: 1901–1910, 2005.

Available online at www.sciencedirect.com
ScienceDirect
Biochemical and Biophysical Research Communications 366 (2008) 174–179
BBRC
www.elsevier.com/locate/ybbrc

Localization of mouse mitochondrial SIRT proteins: Shift of SIRT3 to nucleus by co-expression with SIRT5

Yasuhiko Nakamura, Masahito Ogura, Daisuke Tanaka, Nobuya Inagaki *

Department of Diabetes and Clinical Nutrition, Graduate School of Medicine, Kyoto University, 54 Kawahara-cho, Shogoin, Sakyo-ku, Kyoto 606-8507, Japan

Received 13 November 2007
Available online 3 December 2007

Abstract

Yeast silent information regulator 2 (SIR2) is involved in extension of yeast longevity by calorie restriction, and SIRT3, SIRT4, and SIRT5 are mammalian homologs of SIR2 localized in mitochondria. We have investigated the localization of these three SIRT proteins of mouse. SIRT3, SIRT4, and SIRT5 proteins were localized in different compartments of the mitochondria. When SIRT3 and SIRT5 were co-expressed in the cell, localization of SIRT3 protein changed from mitochondria to nucleus. These results suggest that the SIRT3, SIRT4, and SIRT5 proteins exert distinct functions in mitochondria. In addition, the SIRT3 protein might function in nucleus.

Keywords: SIRT3; SIRT4; SIRT5; Intramitochondrial localization; Localization shift

Silent information regulator 2 (SIR2) is the enzyme that catalyzes NAD^+-dependent protein deacetylation and produces nicotinamide and *O*-acetyl-ADP-ribose [1,2], and is localized in nucleus [3]. In yeast, lifespan is prolonged in low glucose condition [4,5], but such lifespan extension is abolished by SIR2 gene disruption [6], suggesting that SIR2 plays an important role in determining yeast longevity. In mammals, there are seven SIR2 homologs, SIRT1–7 [7]. However, it remains unclear whether SIRTs mediate lifespan extension by calorie restriction.

Human SIRT3, SIRT4, and SIRT5 proteins are known to be localized in mitochondria [7,8]. Mouse SIRT4 was previously shown *in vivo* to ADP-ribosylate glutamate dehydrogenase and down-regulate its activity in pancreatic islets, inhibiting amino acid-stimulated insulin secretion [9]. On the other hand, recent studies have demonstrated that human SIRT3 deacetylates acetyl-CoA synthetase 2 in mitochondrial matrix *in vitro* [10,11]. Human SIRT5 has been shown to have weak deacetylase activity *in vitro* [12]. However, the function of SIRT3 and SIRT5 *in vivo* is still unknown.

Although human SIRT4 and SIRT5 proteins have been reported to localize in mitochondria, precise localization of these proteins is unknown. Regarding SIRT3, localization of SIRT3 protein has been reported to differ in mouse and human, in mitochondrial inner membrane in mouse [13] and in mitochondrial matrix in human [14]. Furthermore, there has been no report on the interaction of the three SIRT proteins known to be localized in mitochondria.

In the present study, we determined localization of mouse SIRT3, SIRT4, and SIRT5 proteins in COS7 cells in different compartments of mitochondria: inner membrane, matrix, and intermembrane space. In addition, we demonstrate that localization of SIRT3

Abbreviations: SIR2, silent information regulator 2; MTS, mitochondrial targeting signal; NLS, nuclear localization signal; GAPDH, glyceraldehyde 3-phosphate dehydrogenase; PNS, post-nuclear supernatant; PHB, prohibitin; ER, estrogen receptor.

* Corresponding author. Fax: +81 75 771 6601.
E-mail address: inagaki@metab.kuhp.kyoto-u.ac.jp (N. Inagaki).

0006-291X/$ - see front matter © 2007 Elsevier Inc. All rights reserved.
doi:10.1016/j.bbrc.2007.11.122

protein in COS7 cells changes from mitochondria to nucleus when co-expressed with SIRT5. We also address the regulatory mechanism of SIRT3 localization by a mutagenesis study of the putative mitochondrial targeting signal (MTS) and nuclear localization signal (NLS).

Materials and methods

Antibodies. The antibodies used for confocal microscopic analysis and Western blot analysis included anti-myc (Santa Cruz Biotechnology), anti-FLAG (Sigma), anti-hsp60 (BD Biosciences), anti-calnexin (Stressgen), anti-glyceraldehyde 3-phosphate dehydrogenase (GAPDH) (Santa Cruz Biotechnology), anti-cytochrome *c* (Cell Signaling), and anti-laminA/C (Cell Signaling).

Plasmid construction. The expression vector for SIRT3-myc, SIRT4-myc, SIRT4-FLAG, and SIRT5-FLAG was constructed as follows. The coding region of SIRT cDNAs was cloned by PCR using mouse liver cDNA. The PCR fragments were subcloned into the pcDNA3.1/myc-His A expression vector (Invitrogen) or the pFLAG-CMV-5a expression vector (Sigma). SIRT3nu and SIRT3mt mutants were constructed by overlap extension PCR method [15] using pcDNA3.1/myc-His-SIRT3 plasmid as the template.

Cell culture and transfection. COS7 cells were maintained in Dulbecco's modified Eagle's medium (Sigma) supplemented with 10% fetal bovine serum (Gibco) in an atmosphere of 5% CO_2 at 37 °C. DNA transfection was performed according to the manufacturer's instructions using FuGene6 Transfection Reagent (Roche). One microgram of plasmid DNA was transfected to COS7 cells in a 3.5-cm dish.

Confocal microscopy. Fluorescence microscopic analysis was performed as described previously [16]. Briefly, COS7 cells transfected with SIRT expression plasmids were fixed and labeled with anti-myc monoclonal IgG and Alexa488-conjugated anti-mouse IgG (Molecular Probes) or anti-FLAG polyclonal IgG and Cy3-conjugated anti-rabbit IgG (Sigma). Fluorescent images were taken and analyzed using a confocal laser microscope (LSM510 META; Carl Zeiss).

Fractionation of post-nuclear supernatant. Fractionation of post-nuclear supernatant was performed as described previously [17]. Twenty micrograms of plasmid DNA was transfected to COS7 cells in a 10-cm dish. The transfected cells were harvested and disrupted in isotonic buffer (PBS containing 0.2 M mannitol, 0.07 M sucrose, and 1 mM EDTA) containing protease inhibitors (Complete, EDTA Free; Roche) with potter homogenizer, followed by centrifuged at 800*g* at 4 °C for 10 min to obtain post-nuclear supernatant (PNS). PNS was centrifuged at 10,000*g* at 4 °C for 10 min to obtain the mitochondria-enriched precipitate fraction. The supernatant was centrifuged at 100,000*g* at 4 °C for 30 min to separate the microsome-enriched precipitate and supernatant fractions. The subcellular fractions were separated by SDS–PAGE and then analyzed by Western blotting.

Alkaline treatment of mitochondria. Mitochondria were prepared from the COS7 cells expressing each SIRT protein, and treated with 100 mM Na_2CO_3 in 10 times volume of mitochondria suspension for 1 h on ice. The reaction mixtures were centrifuged at 100,000*g* at 4 °C for 30 min to separate the precipitate and supernatant fractions. The fractions were subjected to SDS–PAGE followed by Western blot analysis.

Submitochondrial fractionation. The mitochondria were treated with either H_2O or 2% TX-100 in 10 times volume of mitochondria suspension on ice for 1 h, and then treated with 50 μg/ml trypsin on ice for 1 h. The reaction mixtures were separated by SDS–PAGE and then analyzed by Western blotting.

Subcellular fractionation using digitonin. The transfected COS7 cells were harvested and lysed with PBS containing 2% digitonin. The cell lysate was centrifuged at 800*g* at 4 °C for 10 min to obtain nucleus-enriched insoluble and soluble fractions. The fractions were separated by SDS–PAGE and then analyzed by Western blotting.

Results and discussion

Distinct localizations of SIRT3, SIRT4, and SIRT5 in mitochondria

To determine the intracellular localization of mouse SIRT3, SIRT4, and SIRT5 proteins, expression plasmid encoding each of these SIRT proteins fused with myc tag or FLAG tag at the C terminus was transfected into COS7 cells. The SIRT proteins were stained with anti-myc antibody or anti-FLAG antibody and its intracellular localization was examined using confocal microscopy (Fig. 1A). All three images of SIRT3, SIRT4, and SIRT5 proteins merged well with that of MitoTracker Red, a marker of mitochondria, indicating that all of these SIRT proteins are localized in mitochondria. Cell fractionation was then performed using cells transfected with the SIRT expression plasmids. PNS of the cells was centrifuged and fractionated into the mitochondria-enriched low-speed precipitate (P1), the microsome-enriched high-speed precipitate (P2), and the supernatant (S) fractions (Fig. 1B). All of the three SIRT proteins were found in the P1 fraction as was hsp60 protein, a marker of mitochondria, affirming their localization in mitochondria.

To clarify localization of the three SIRT proteins in mitochondria, mitochondrial fraction prepared from COS7 cells expressing each of the SIRT proteins was treated with Na_2CO_3 and centrifuged. SIRT3 protein was detected in the precipitate fraction, while SIRT4 and SIRT5 proteins were detected in the supernatant fraction, indicating that SIRT3 protein is integrated into either mitochondrial outer or inner membrane and that SIRT4 and SIRT5 are soluble and not membrane proteins (Fig. 1C). After treating the mitochondrial fractions with either H_2O or TX-100, the fractions were treated with trypsin. When mitochondria are treated with H_2O, the mitoplast can be obtained. SIRT3 and SIRT5 proteins were digested with trypsin in both H_2O- and TX-100-treated mitochondria but were not digested in untreated mitochondria (Fig. 1D), indicating that these proteins are localized either in intermembrane space or in inner membrane. In contrast, SIRT4 was digested only in the TX-100-treated mitochondria. Taken together, these results indicate that SIRT3, SIRT4, and SIRT5 proteins are localized in inner membrane, matrix, and intermembrane space, respectively, in mitochondria. In human, SIRT3 protein was reported to localize in mitochondrial matrix [14]. Since mouse SIRT3 protein lacks a region corresponding to the N-terminal 142-amino acid residues of human SIRT3 protein, the region could be critical in determining localization in mitochondria. In addition, the function of SIRT3 might differ in humans and mice.

SIRT3 is localized in nucleus when co-expressed with SIRT5

We then examined localization of these three mitochondrial SIRT proteins when two of them were co-expressed in

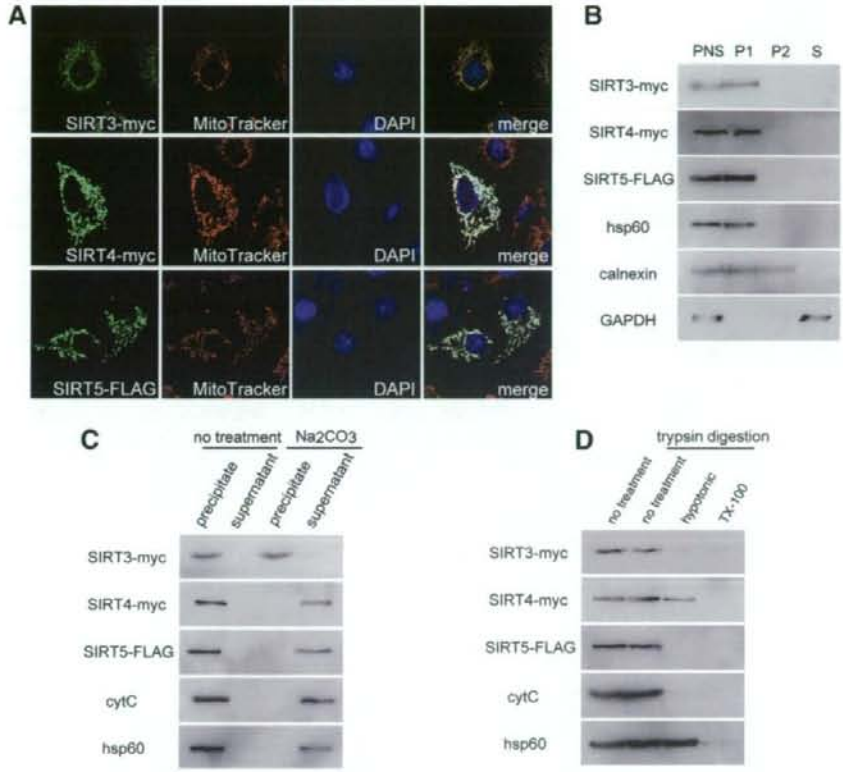

Fig. 1. Localization of SIRT3, SIRT4, and SIRT5 in mitochondria. (A) Confocal microscopy. SIRT3-myc (upper panels), SIRT4-myc (middle panels), and SIRT5-FLAG (lower panels) were expressed in COS7 cells and immunostained with anti-myc antibody or anti-FLAG antibody. Mitochondria and nuclei were stained by MitoTracker Red and DAPI, respectively, and fluorescent images were obtained using a confocal microscope. (B) Fractionation of post-nuclear supernatant. SIRT3-myc, SIRT4-myc, and SIRT5-FLAG proteins each was expressed in COS7 cells, and the obtained PNS was fractionated into mitochondria-enriched precipitate (P1), microsome-enriched precipitate (P2), and supernatant (S) fractions. The three fractions were separated by SDS–PAGE and then analyzed by Western blotting using anti-myc antibody for SIRT3-myc and SIRT4-myc or anti-FLAG antibody for SIRT5-FLAG. Hsp60, calnexin, and GAPDH were used as endogenous markers for mitochondria, microsome, and cytosol, respectively. (C) Alkaline treatment of mitochondria. Mitochondria prepared from the COS7 cells expressing each of the SIRT3-myc, SIRT4-myc, and SIRT5-FLAG proteins were treated with Na_2CO_3. The reaction mixture was centrifuged to separate the precipitate and supernatant fractions, containing membrane-integrated proteins and soluble proteins, respectively. The two fractions were analyzed by Western blotting. Cytochrome *c* (cyt*c*) and hsp60 were used as endogenous protein markers for mitochondrial soluble protein. (D) Submitochondrial fractionation. The mitochondria from COS7 cells expressing one of three SIRT proteins were treated with either H_2O (hypotonic) or TX-100, and then treated with trypsin. The reaction mixtures were analyzed by Western blotting. Cytochrome *c* and hsp60 were used as endogenous markers for mitochondrial intermembrane space protein and matrix protein, respectively.

COS7 cells (Fig. 2A). When SIRT3 and SIRT5 proteins were co-expressed, the localization of SIRT3 protein but not SIRT5 protein changed from mitochondria to nucleus (upper panels). However, SIRT proteins remained in mitochondria with the other combinations of co-expression (SIRT3 and SIRT4, middle panels, and SIRT4 and SIRT5, lower panels). To confirm the localization shift of SIRT3 protein by co-expression with SIRT5, we performed fractionation of PNS (Fig. 2B). SIRT5 protein appears in P1 fraction, indicating its localization in mitochondria. In contrast, SIRT3 protein is not found in PNS but appears in whole cell lysate, indicating that SIRT3 is localized in nucleus. These results are consistent with confocal microscopic study. In addition, we performed another cell fractionation to separate nucleus and the remaining portion of the cell using digitonin (Fig. 2C). The nuclear proteins lamin A/C appeared in insoluble (INS) fraction and the mitochondrial protein hsp60 occurred in both insoluble and soluble (SOL) fractions to a similar extent. SIRT3 protein also was detected in both insoluble and soluble fractions to a similar extent when expressed alone. However, the majority of SIRT3 protein was detected in the insoluble fraction when co-expressed with SIRT5, further confirming the localization shift of SIRT3 protein from mitochondria to nucleus. Taken together, we clearly show here for the first time that the intracellular localization of SIRT3 protein changes from mitochondria to nucleus in the presence of SIRT5, suggesting that SIRT3 plays a role as a regulator of nuclear proteins through its deacetylase or other, unknown activity.

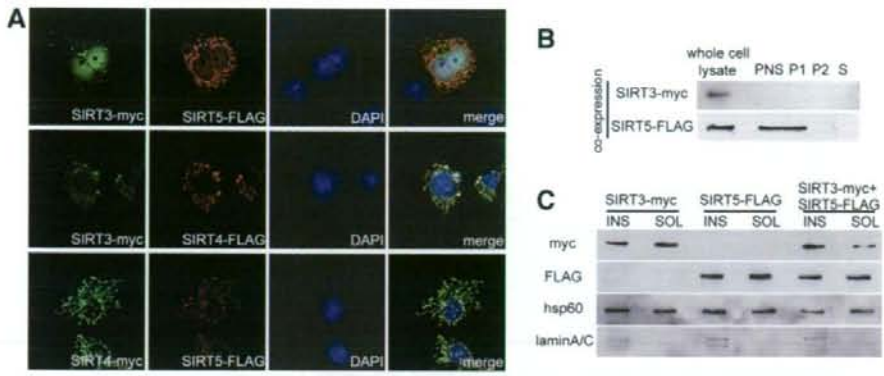

Fig. 2. Localization of SIRT3 when co-expressed with SIRT5. (A) Confocal microscopic analysis of COS7 cells expressing two of the three mitochondrial SIRT proteins. SIRT3-myc and SIRT5-FLAG (upper panels), SIRT3-myc and SIRT4-FLAG (middle panels), and SIRT4-myc and SIRT5-FLAG (lower panels) were co-expressed in COS7 cells, and immunostained using antibodies against myc tag and FLAG tag. Nuclei were stained by DAPI. (B) Subcellular fractionation of PNS. PNS of COS7 cells co-expressing SIRT3-myc and SIRT5-FLAG was fractionated into mitochondria-enriched precipitate (P1), microsome-enriched precipitate (P2), and supernatant (S) fractions, and these fractions along with whole cell lysate were analyzed by Western blotting. (C) Subcellular fractionation using digitonin. COS7 cells expressing either SIRT3-myc (left) or SIRT5-FLAG (middle) or both (right) were solubilized by digitonin, and the obtained lysate was centrifuged and fractionated into nuclear-enriched insoluble (INS), and soluble (SOL) fractions. Hsp60 and laminA/C were used as endogenous markers for mitochondria protein and nucleus protein, respectively.

Disruption of putative mitochondrial targeting signal of SIRT3

Because the segment containing amino acid residues 66–88 potentially forms a basic amphiphilic α-helical structure, it could serve as a MTS. To examine the role of this segment, SIRT3 mutant SIRT3mt, in which the four amino acid residues 72–75 were replaced by four alanine residues, was constructed (Fig. 3A). When SIRT3mt alone was expressed in COS7 cells, SIRT3mt protein was not detected in mitochondria but was widely distributed in the cell in confocal microscopic analysis (Fig. 3B, upper panels). In addition, when SIRT3mt and SIRT5 were co-expressed, the distribution of SIRT3mt protein was not changed compared to that expressed alone (Fig. 3B, lower panels). In fractionation of PNS, SIRT3mt protein was fractionated into S fraction both when SIRT3mt was expressed alone and when SIRT3mt and SIRT5 were co-expressed. SIRT5 protein was localized in mitochondria when SIRT3mt and SIRT5 were co-expressed (Fig. 3C). These results indicate that the MTS is necessary not only for targeting SIRT3 to mitochondria in the absence of SIRT5 but also for targeting SIRT3 to nucleus in the presence of SIRT5.

Disruption of putative nuclear localization signal of SIRT3

We found that the sequence containing amino acid residues 213–219 of the SIRT3 protein closely resembles the

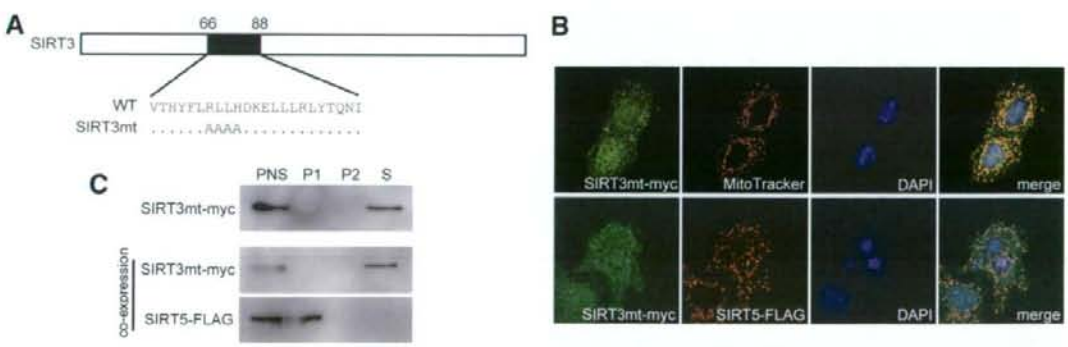

Fig. 3. Effect of disruption of putative mitochondrial targeting signal of SIRT3. (A) Alanine replacement of putative MTS of SIRT3. Four residues of the putative MTS of SIRT3 (amino acid residues 72–75) were replaced with four alanine residues. In the SIRT3mt sequence, amino acid residues identical with wild-type SIRT3 protein are indicated with dots. (B) Confocal microscopy. Immunofluorescent images of COS7 cells expressing SIRT3mt-myc alone (upper panels) or both SIRT3mt-myc and SIRT5-FLAG (lower panels) are shown. Mitochondria and nuclei were stained by MitoTracker Red and DAPI, respectively. (C) Subcellular fractionation of PNS. PNSs of COS7 cells expressing SIRT3mt-myc alone (an upper panel) or co-expressing SIRT3mt-myc and SIRT5-FLAG (middle and lower panels) were centrifuged and fractionated into mitochondria-enriched precipitate (P1), microsome-enriched precipitate (P2), and supernatant (S) fractions. The fractions were analyzed by Western blotting.

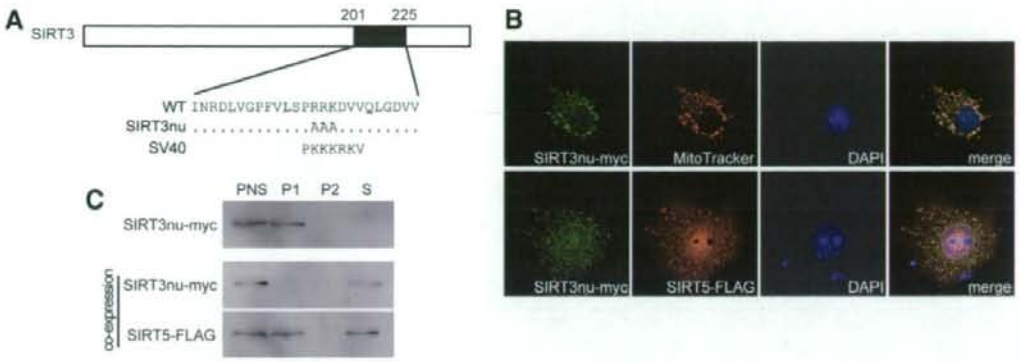

Fig. 4. Effect of disruption of putative nuclear localization signal of SIRT3. (A) Comparison of the amino acid sequences of putative NLS of SIRT3, SIRT3nu, and SV40 large T antigen. Three basic amino acid residues of the putative NLS of SIRT3 (amino acid residues 214–216) were replaced with three alanine residues. In the SIRT3nu sequence, amino acid residues identical with wild-type SIRT3 protein are indicated with dots. The classical NLS of SV40 large T antigen also is shown (SV40). (B) Confocal microscopy. Immunofluorescent images of COS7 cells expressing SIRT3nu-myc alone (upper panels) or both SIRT3nu-myc and SIRT5-FLAG (lower panels) are shown. Mitochondria and nuclei were stained by MitoTracker Red and DAPI, respectively. (C) Subcellular fractionation of PNS. PNSs of the COS7 cells expressing SIRT3nu-myc alone (an upper panel) or co-expressing SIRT3nu-myc and SIRT5-FLAG (middle and lower panels) were fractionated into mitochondria-enriched precipitate (P1), microsome-enriched precipitate (P2), and supernatant (S) fractions. The fractions were analyzed by Western blotting.

classical NLS of the SV40 T antigen (Fig. 4A). To examine whether this sequence functions as a NLS, the mutant SIRT3 protein SIRT3nu, in which the three basic amino acid residues (214–216) in the putative NLS of SIRT3 were replaced by three alanine residues (Fig. 4A), was constructed. When SIRT3nu alone was expressed in COS7 cells, it was localized in mitochondria (Fig. 4B, upper panels). In the cells co-expressing SIRT3nu and SIRT5, a shift of SIRT3nu protein to the nucleus was not observed, and SIRT3nu protein and a part of SIRT5 protein were scattered widely in the cell in confocal microscopic analysis (Fig. 4B, lower panels). In fractionation of PNS, all of the SIRT3nu protein and nearly half of the SIRT5 protein were shifted from P1 fraction to S fraction by co-expression (Figs. 1B and 4C). These results suggest that the segment containing amino acid residues 213–219 of SIRT3 plays an important role in the localization shift of SIRT3 protein to nucleus when co-expressed with SIRT5. Furthermore, SIRT5 may well hamper SIRT3nu localization in mitochondria through interaction with SIRT3nu. However, further study is required to elucidate the mechanism of the localization shift of SIRT3 protein.

Interestingly, recent study has reported that human prohibitin 2 (PHB2), known as a repressor of estrogen receptor (ER) activity, is localized in the mitochondrial inner membrane, and translocates to the nucleus in the presence of ER and estradiol [18]. Although the mechanism of regulation of the expression level of SIRT5 remains unknown, SIRT3 might play a role in communication between nucleus and mitochondria in a SIRT5-dependent manner.

The function of mitochondrial SIRT proteins is still not well known. In the present study, we determined the exact localization of mouse SIRT3, SIRT4, and SIRT5 proteins in mitochondria. In addition, we demonstrated that SIRT3 can be present in nucleus in the presence of SIRT5. It has been reported that SIRT3 deacetylates proteins that are not localized in mitochondria *in vitro* such as histone-4 peptide and tubulin [14]. Thus, if SIRT3 is present in nucleus *in vivo*, SIRT3 protein might well deacetylate nuclear proteins. These results provide useful information for the investigation of the function of these proteins.

Acknowledgments

This work was supported by Scientific Research Grants and a Grant-in-Aid for Creative Scientific Research 15GS0301 from the Ministry of Education, Culture, Sports, Science, and Technology of Japan.

References

[1] J.C. Tanny, G.J. Dowd, J. Huang, H. Hilz, D. Moazed, An enzymatic activity in the yeast Sir2 protein that is essential for gene silencing, Cell 99 (1999) 735–745.
[2] S. Imai, C.M. Armstrong, M. Kaeberlein, L. Guarente, Transcriptional silencing and longevity protein Sir2 is an NAD-dependent histone deacetylase, Nature 403 (2000) 795–800.
[3] M. Gotta, S. Strahl-Bolsinger, H. Renauld, T. Laroche, B.K. Kennedy, M. Grunstein, S.M. Gasser, Localization of Sir2p: the nucleolus as a compartment for silent information regulators, EMBO J. 16 (1997) 3243–3255.
[4] I. Muller, M. Zimmermann, D. Becker, M. Flomer, Calendar life span versus budding life span of *Saccharomyces cerevisiae*, Mech. Aging Dev. 12 (1980) 47–52.
[5] S.J. Lin, M. Kaeberlein, A.A. Andalis, L.A. Sturtz, P.A. Defossez, V.C. Culotta, G.R. Fink, L. Guarente, Calorie restriction extends *Saccharomyces cerevisiae* lifespan by increasing respiration, Nature 418 (2002) 344–348.
[6] S.J. Lin, P.A. Defossez, L. Guarente, Requirement of NAD and SIR2 for life-span extension by calorie restriction in *Saccharomyces cerevisiae*, Science 289 (2000) 2126–2128.

[7] E. Michishita, J.Y. Park, J.M. Burneskis, J.C. Barrett, I. Horikawa, Evolutionarily conserved and nonconserved cellular localizations and functions of human SIRT proteins, Mol. Biol. Cell 16 (2005) 4623–4635.
[8] P. Onyango, I. Celic, J.M. McCaffery, J.D. Boeke, A.P. Feinberg, SIRT3, a human SIR2 homologue, is an NAD-dependent deacetylase localized to mitochondria, Proc. Natl. Acad. Sci. USA 99 (2002) 13653–13658.
[9] M.C. Haigis, R. Mostoslavsky, K.M. Haigis, K. Fahie, D.C. Christodoulou, A.J. Murphy, D.M. Valenzuela, G.D. Yancopoulos, M. Karow, G. Blander, C. Wolberger, T.A. Prolla, R. Weindruch, F.W. Alt, L. Guarente, SIRT4 inhibits glutamate dehydrogenase and opposes the effects of calorie restriction in pancreatic β cells, Cell 126 (2006) 941–954.
[10] B. Schwer, J. Bunkenborg, R.O. Verdin, J.S. Andersen, E. Verdin, Reversible lysine acetylation controls the activity of the mitochondrial enzyme acetyl-CoA synthetase 2, Proc. Natl. Acad. Sci. USA 103 (2006) 10224–10229.
[11] W.C. Hallows, S. Lee, J.M. Denu, Sirtuins deacetylate and activate mammalian acetyl-CoA synthetases, Proc. Natl. Acad. Sci. USA 103 (2006) 10230–10235.
[12] B.J. North, B.L. Marshall, M.T. Borra, J.M. Denu, E. Verdin, The human Sir2 ortholog, SIRT2, is an NAD^+-dependent tubulin deacetylase, Mol. Cell 11 (2003) 437–444.
[13] T. Shi, F. Wang, E. Stieren, Q. Tong, SIRT3, a mitochondrial sirtuin deacetylase, regulates mitochondrial function and thermogenesis in brown adipocytes, J. Biol. Chem. 280 (2005) 13560–13567.
[14] B. Schwer, B.J. North, R.A. Frye, M. Ott, E. Verdin, The human silent information regulator (Sir)2 homologue hSIRT3 is a mitochondrial nicotinamide adenine dinucleotide-dependent deacetylase, J. Cell Biol. 158 (2002) 647–657.
[15] S.N. Ho, H.D. Hunt, R.M. Horton, J.K. Pullen, L.R. Pease, Site-directed mutagenesis by overlap extension using the polymerase chain reaction, Gene 77 (1989) 51–59.
[16] Y. Matsumura, N. Ban, K. Ueda, N. Inagaki, Characterization and classification of ATP-binding cassette transporter ABCA3 mutants in fatal surfactant deficiency, J. Biol. Chem. 281 (2006) 34503–34514.
[17] Y. Nakamura, H. Suzuki, M. Sakaguchi, K. Mihara, Targeting and assembly of rat mitochondrial translocase of outer membrane 22 (TOM22) into the TOM complex, J. Biol. Chem. 279 (2004) 21223–21232.
[18] K. Kasashima, E. Ohta, Y. Kagawa, H. Endo, Mitochondrial functions and estrogen receptor-dependent nuclear translocation of pleiotropic human prohibitin 2, J. Biol. Chem. 281 (2006) 36401–36410.

DIABETES RESEARCH AND CLINICAL PRACTICE 81 (2008) 284–289

available at www.sciencedirect.com

ScienceDirect

journal homepage: www.elsevier.com/locate/diabres

Factors responsible for elevation of 1-h postchallenge plasma glucose levels in Japanese men

Norio Harada [a], *Mitsuo Fukushima* [a,b,*], *Kentaro Toyoda* [a], *Rie Mitsui* [a], *Tomoyo Izuka* [b], *Ataru Taniguchi* [c], *Yoshikatsu Nakai* [d], *Yuichiro Yamada* [a], *Yutaka Seino* [a,c], *Nobuya Inagaki* [a]

[a] *Department of Diabetes and Clinical Nutrition, Graduate School of Medicine, Kyoto University, Kyoto, Japan*
[b] *Health Informatics Research Group, Foundation for Biomedical Research and Innovation, 1-5-4 Minatojima-minami-machi, Chuo-ku, Kobe, Hyogo 650-0047, Japan*
[c] *Division of Diabetes and Clinical nutrition, Kansai Electric Power Hospital, Osaka, Japan*
[d] *Karasuma-Oike Nakai Clinic, Kyoto, Japan*

ARTICLE INFO

Article history:
Received 31 January 2008
Accepted 16 April 2008
Published on line 31 July 2008

Keywords:
1-h postchallenge plasma glucose level (1-h PG)
Insulinogenic index
Insulin secretion
Insulin sensitivity

ABSTRACT

The 1-h postchallenge plasma glucose (1-h PG) level is considered to be a good index of the development of glucose intolerance and type 2 diabetes as well as of diabetic complications. In some cases, in Japanese, 1-h PG is elevated despite normal fasting glucose during oral glucose tolerance test (OGTT), but the factors responsible remain unclear. In the present study, subjects with normal glucose tolerance (NGT), isolated impaired fasting glucose (IFG), and isolated impaired glucose tolerance (IGT) were divided into subgroups at 1-h PG of 10.0 mM, and the four indices of insulin secretion and insulin sensitivity were compared. In all three categories, the insulinogenic index in subjects with elevated 1-h PG was remarkably lower than in those without elevated 1-h PG. In addition, the insulinogenic index was the strongest factor in elevated 1-h PG according to the multiple regression analysis. Interestingly, one third of the NGT subjects enrolled in this study had elevated 1-h PG. These subjects showed significantly elevated area under the curve of glucose (G-AUC) compared to NGT subjects without 1-h PG elevation. Thus, elevated 1-h PG in Japanese subjects indicates mildly impaired glucose tolerance due to decreased early-phase insulin secretion.

1. Introduction

Type 2 diabetes is characterized by both decreased insulin secretion and reduced insulin sensitivity [1–3]. Some patients with glucose intolerance leading to type 2 diabetes show elevated postchallenge plasma glucose without elevated fasting glucose during oral glucose tolerance test (OGTT) [4–6]. Although elevated 1-h postchallenge plasma glucose involves a different regulatory mechanism than 2-h postchallenge plasma glucose (2-h PG), 1-h postchallenge plasma glucose (1-h PG) is also as reliable an index of glucose tolerance as 2-h PG generally [7,8]. However, the relevance of 1-h PG and 2-h PG for diabetes screening is controversial [9,10]. It has been reported that subjects with 1-h PG higher than 10.0 mmol/l show higher risk of developing diabetes than subjects with lower 1-h PG [11]. In addition, 1-h PG higher than 11.2 mmol/l was found to be an independent risk factor for mortality in cardiovascular disease [12–14]. It was recommended in a

* *Corresponding author at*: Health Informatics Research Group, Foundation for Biomedical Research and Innovation, 1-5-4 Minatojima-minami-machi, Chuo-ku, Kobe, Hyogo 650-0047, Japan. Tel.: +81 78 304 5988; fax: +81 78 304 5989.
E-mail address: fukum@tri-kobe.org (M. Fukushima).
0168-8227/$ – see front matter
doi:10.1016/j.diabres.2008.04.011